Advances in Applied Energy 12 (2023) 100154

Contents lists available at ScienceDirect

Advances in Applied Energy

journal homepage: www.elsevier.com/locate/adapen

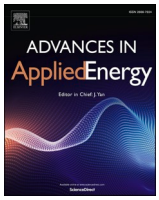

Experimental research and multi-physical modeling progress of Zinc-Nickel single flow battery: A critical review

Xinyu Huang [a], Rui Zhou [b], Xilian Luo [a], Xiaohu Yang [a,*], Jie Cheng [c], Jinyue Yan [d,e,*]

[a] Institute of the Building Environment & Sustainability Technology, School of Human Settlements and Civil Engineering, Xi'an Jiaotong University, Xi'an 710049, China
[b] State Key Laboratory of Solid Lubrication, Lanzhou Institute of Chemical Physics, Chinese Academy of Sciences, Lanzhou 730000, China
[c] Zhejiang Yuyuan Energy Storage Technology Co. Ltd., Huzhou 313100, China
[d] Department of Building Environment and Energy Engineering, The Hong Kong Polytechnic University, Kowloon, Hong Kong, China
[e] Future Energy Profile, School of Business, Society and Engineering, Mälardalen University, Västerås, Sweden

ARTICLE INFO

Keywords:
Zinc–Nickel single flow battery
Experimental optimization
Numerical analysis
Loss of polarization
Side effects

ABSTRACT

Electrochemical energy storage technologies hold great significance in the progression of renewable energy. Within this specific field, flow batteries have emerged as a crucial component, with Zinc–Nickel single flow batteries attracting attention due to their cost-effectiveness, safety, stability, and high energy density. This comprehensive review aims to thoroughly evaluate the key concerns and obstacles associated with this type of battery, including polarization loss, hydrogen evolution reaction, and dendrite growth, among others. Additionally, the study highlights ongoing research endeavors focused on addressing these concerns, such as optimizing battery operating conditions and developing new electrodes. Furthermore, recent advancements in experimental processes and multi-scale numerical simulations of Zinc–Nickel single flow batteries, facilitated by the visual literature analysis software VOSviewer, are also explored. The primary objective of this review is to acquire a comprehensive understanding of the electrochemical reaction and internal mass transfer mechanism of Zinc–Nickel single flow batteries, while also anticipating future research directions and prospects.

1. Introduction

The availability of clean and sufficient energy plays a crucial role in promoting sustainable and robust economic growth. However, the rapid expansion of social and economic activities has resulted in a considerable surge in energy demand, creating a rather challenging global energy situation [1,2]. Various energy sources are available, including fossil fuels, nuclear energy, river hydraulic potential energy, and renewable energy [3,4]. Nevertheless, conventional fossil fuel energy sources face significant obstacles, such as the risk of insufficient reserves for future development [5] and the escalating problem of environmental pollution [6]. Renewable energy is gaining significant support due to its abundant resources and lack of pollution. Its proportion in the energy sector is increasing steadily, making large-scale adoption of renewable energy the primary focus of future energy development [7,8]. However, the intermittent nature of renewable energy poses challenges for grid-connected power generation regarding operation, safety, and regulation [9], significantly limiting its practical usage [10]. To address these issues, the development of efficient large-scale energy storage technology offers a solution [11,12]. This technology, such as the development and deployment of solar cells, mitigated short-term output fluctuations and tracked scheduled output but also increased the certainty, predictability, and economics of renewable energy generation from wind/solar [13,14]. Furthermore, it can serve multiple functions such as load tracking, power quality management, peak shaving, valley filling, frequency, and voltage regulation, enhancing the power system's regulation capability [15,16]. Consequently, developing large-scale energy storage technology efficiently is highly significant, and many countries classify it as a strategic cornerstone to support the development of new energy [17,18].

Energy storage technology can be categorized into two types: physical energy storage and chemical energy storage [19]. Physical energy storage includes methods such as pumped storage, compressed air energy storage, and flywheel energy storage. Despite having advantages such as no pollution and long cycle life, physical energy storage often suffers from low energy conversion efficiency, high investment costs, site selection limitations, prolonged construction cycles, long response time, and equipment and material demands [20,21]. Chemical energy storage covers a range of systems, including liquid flow batteries,

* Corresponding authors.
E-mail addresses: xiaohuyang@xjtu.edu.cn (X. Yang), jinyue.yan@mdh.se (J. Yan).

https://doi.org/10.1016/j.adapen.2023.100154
Received 12 July 2023; Received in revised form 15 September 2023; Accepted 16 September 2023
Available online 29 September 2023

Nomenclature

Abbreviation

ZNB	Zinc–Nickel single flow battery
RFB	Redox flow battery
VRFB	all-vanadium redox flow battery
SOC	state of charge
HER	hydrogen evolution reaction
CVA	cyclic voltammetry
OER	oxygen evolution reaction
EIS	electrochemical impedance spectroscopy
CE	Coulomb efficiency
LBM	lattice Boltzmann method
TBAB	tetrabutylammonium bromide
NF	nickel foam
NS	nickel-plated steel strip
RSM	response surface method
PF	phase field
QSGS	quartet structure generation set

Symbols

D_1	diffusion coefficients in proton $Ni(OH)_2$
D_2	diffusion coefficients in proton NiOOH
α_{g,O_2}	volume fraction of oxygen
ε_0	porosity of the positive electrode
p_0	pressure in the standard state
p	partial pressure
c_R^*	surface concentrations of reactants
c_P^*	surface concentrations of products
n	number of electrons transferred
j_0^0	current density in the standard reference state
I	current density

Greeksymbols

α	activity
η	activation over-potential
β	transfer coefficient

Subscripts

d	charging process
t	discharge process

Table 1
Comparison of flow battery technology and performance of different energy storage devices [37].

Energy storage mode	Life cycle (year)	Cycle life (thousands of cycles)	Efficiency (%)	Cost ($/kWh)	limitation
Hydraulic potential energy [38]	30	20–50	70–80	80–200	Special geographical requirements.
Superconducting magnet [39]	30	1–10	90–95	10,000	Short power output time (< 0.25 h).
Compressed air energy storage [40]	30	9–30	60–70	50–110	Special geographical requirements, the existence of high-pressure vessels.
Flywheel energy storage [41]	20	> 20	> 90	300–5000	Low energy density and efficiency.
Lithium-ion battery [42,43]	5–10	5–7	> 90	850–5000	Risk of spontaneous combustion or explosion, high cost.
Supercapacitor [44]	lower	10–100	> 90	82,000	Low energy density and serious self-discharge.
Lead-acid battery [45]	5–10	0.2–1.5	70–76	350–1500	Low energy density and poor deep discharge performance.
Sodium-sulfur battery [46]	5–10	0.021–4.5	85–90	300–950	High temperature operation, there is risk of thermal runaway.
Flow battery [47,48]	> 10	5–14	75–85	180–250	The energy density is moderately low.

lithium-ion batteries, lead-acid batteries, and sodium-sulfur batteries [22,23]. Table 1 compares the performance of different energy storage devices and flow battery technologies. Lithium-ion batteries are prevalent in mobile phones, laptops, electric vehicles, and other devices because of their long cycle life and high energy density [24–26]. However, they are costly to manufacture due to thermal management challenges [27,28]. While the cycle life of a lithium-ion battery reactor system shows room for improvement compared to a single lithium-ion battery [29,30], lead-acid batteries have serious problems with self-discharge and limited cycle life, and improper treatment of lead-containing batteries will cause environmental pollution [31]. The operating temperature of sodium-sulfur batteries needs to be as high as 320 °C [32,33], so the corresponding insulation equipment and temperature control system are required, increasing the battery system's cost and complexity. In addition, damage to ceramic electrolytes can lead to direct contact between liquid sodium and liquid sulfur, resulting in thermal runaway accidents [34]. Flow batteries have emerged as a promising option due to their affordability, long lifespan, and high efficiency [35,36]. Flow batteries have unique advantages over other chemical energy storage technologies due to their independent output power and capacity. The capacity of the battery system is determined by the volume and concentration of the electrolytic liquid containing active substances. At the same time, the power output depends on the number of batteries and the active area of the electrodes.

The most representative all-vanadium flow battery [49,50] serves as an example, using a normal temperature liquid solution as an electrolyte circulating in a loop comprising a liquid storage tank, porous structure electrolytic flow channel, and connecting pipes (as shown in Fig. 1**(a)**). Notably, this battery system is impervious to internal short-circuit failures and heat-induced thermal runaway problems, thereby manifesting elevated safety and reliability standards [51]. Vanadium ions with different valences are electrochemically reacted in solution, preventing significant ion cross-contamination, self-discharge issues, and long life cycles. Moreover, the battery's modular characteristics facilitate a more adaptable reactor system design [52]. However, using ion-exchange membranes increases the cost, and the selective permeability of the membranes during operation modestly reduces the battery's cycle life [53].

In recent years, there has been significant attention given to the development of new flow batteries, such as the Zinc–Nickel single flow battery (ZNB), as shown in Fig. 1**(a)** [54,55]. The ZNB is characterized by several notable features: (1) high cycle life, reaching up to over 10,000 cycles; (2) high safety performance, utilizing an ion exchange membrane and an alkaline water system; (3) large battery capacity, with a single unit capable of reaching over 300 Ah; (4) low cost, adopting a single liquid flow system with moderately priced electrode materials; (5) good environmental performance, utilizing safe, nontoxic, and pollution-free materials; (6) a wide range of operating temperatures from -40 °C to 40 °C, thereby contributing to the efficient operation and other advantages for batteries [56,57].

ZNB, a potential sedimentation single flow battery, shows promise as a future liquid-flow energy storage battery technology. However, there

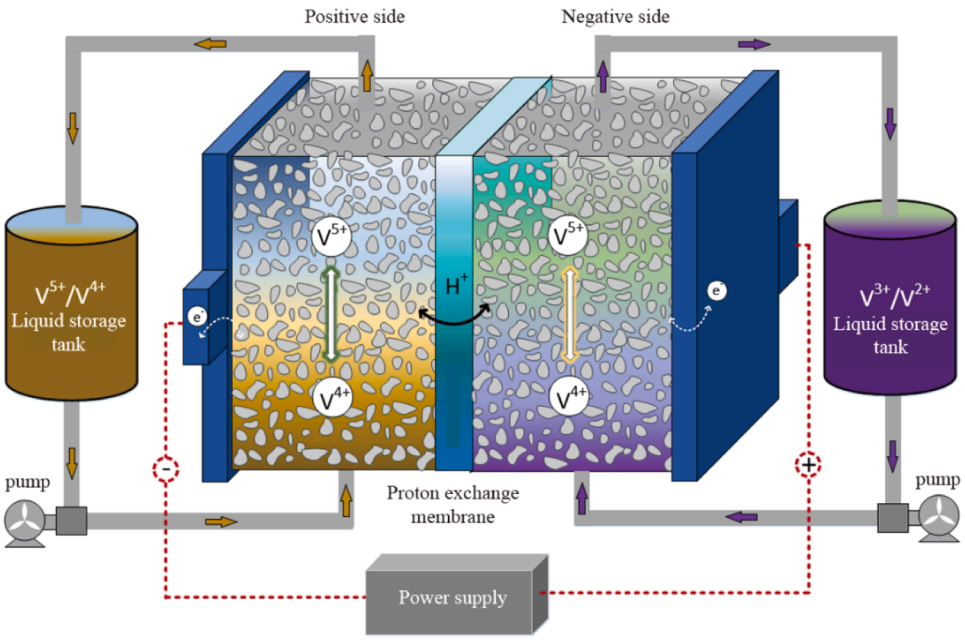

(a)

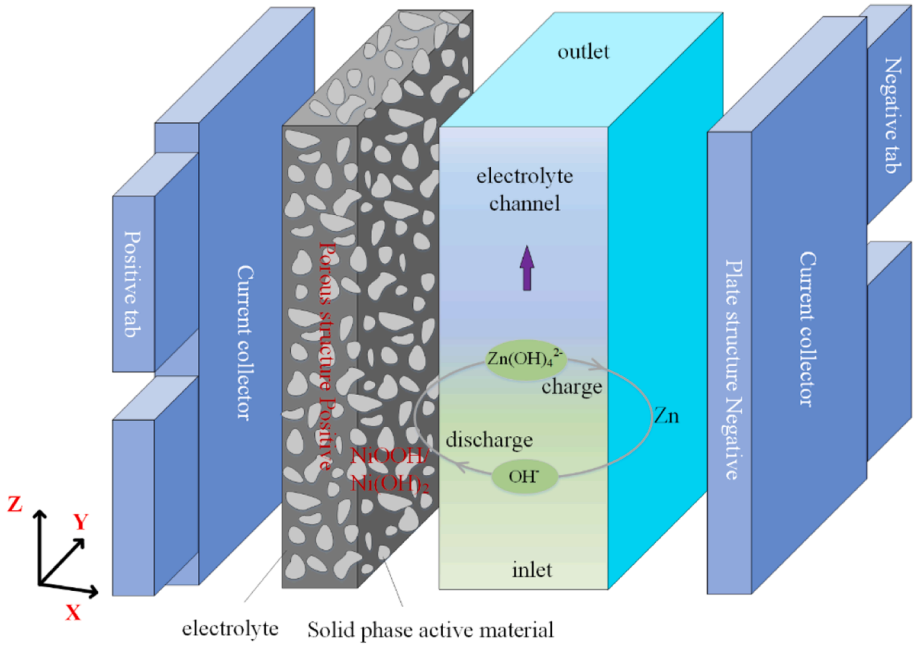

(b)

Fig. 1. Internal reaction diagram of batteries: (a) all-vanadium flow battery; (b) Zinc–Nickel single flow battery.

are common challenges faced by settlement flow batteries, including ZNB, such as low energy density, capacity attenuation due to side reactions, and battery failure caused by dendrite growth. This paper aims to provide a scholarly review of current experimental and numerical studies on the ZNB. The objective is to enhance its energy density and cycle life and comprehensively understand the interaction mechanism between the electrochemical reaction and mass transfer process of the ZNB system. The ultimate goal is to establish a theoretical foundation for inhibiting side reactions and optimizing the structure of the ZNB from a mass transfer standpoint. This research endeavors to facilitate the further industrialization and development of the ZNB system.

2. Current status of flow battery research

Redox flow batteries (RFBs) were first introduced by NASA in 1974 [58]. This technology utilizes reversible redox reactions to convert active substances in the electrolyte between positive and negative electrodes into electric and chemical energy. RFBs can be categorized into double- and single-flow systems based on the battery structure [59, 60]. In a double-flow system, two different electrolytes are isolated by

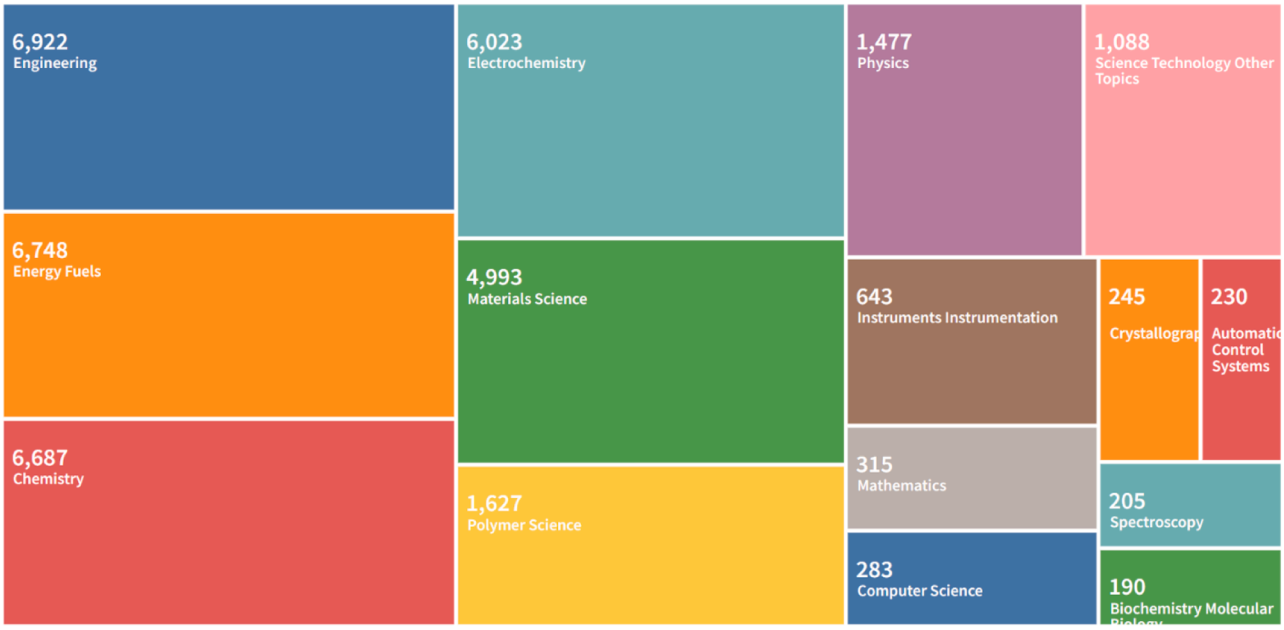

Fig. 2. (a) Search the scientific categories covered by ZNB related literature; (b) Number of published papers and citations on ZNB since 2010; (c) The top 10 journals in terms of number of articles published; (d) Visualization analysis of keywords in 2298 literatures on RFBs in recent three years (occurrence times greater than 100).

an exchange membrane that flows through the passage. This category includes various types of RFBs, such as all-vanadium, iron-chromium, and all-iron flow batteries. In contrast, the single-flow system is characterized by a simpler structure. Examples of RFBs in this system include double-deposition flow batteries, metal-air flow batteries (such as all-lead deposition, aluminum-air, and zinc-air flow batteries), and single-deposit flow cells (such as ZNB, PbO_2/Zn single-flow batteries, and so on).

This review comprehensively examines 8955 articles pertaining to RFBs since 2010. These articles were sourced from the top 10 journals and were classified based on their scientific focus, number of publications, and citations, as depicted in Figs. 2**(a), (b)**, and **(c)**, respectively. Fig. 2**(a)** depicts the results of the literature analysis based on "research direction" sourced from the Web of Science database. It is apparent that RFBs' research topics predominantly include "Engineering", "Energy Fuels", "Chemistry", "Electrochemistry", and "Materials Science". Specifically, there are 5362 research papers, 521 review papers, and 597 conference papers. Fig. 2**(b)** displays the number of published papers and citations after 2010, with 71,186 retrieval instances for the 8955 papers. Published papers and citations witness annual upsurges, leading to the maximum number of 1119 published papers in 2022 and 204,290 citations in 2021. The citation frequency for each paper is 22.81, showcasing close linkages to renewable energy and energy storage technology development. Fig. 2**(c)** highlights the top 10 journals in the RFB field. Currently, the three leading journals are "Journal of Power Sources", "Journal of the Electrochemical Society", and "Electrochimica

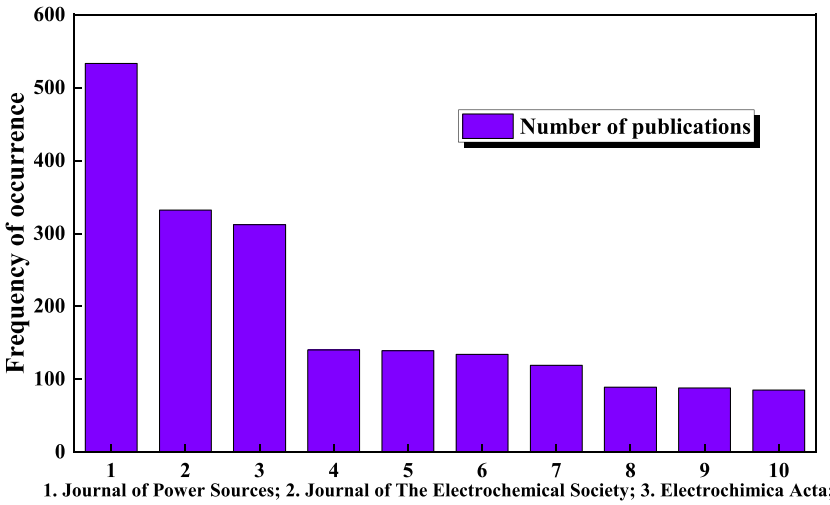

1. Journal of Power Sources; 2. Journal of The Electrochemical Society; 3. Electrochimica Acta;
4. Journal of Materials Chemistry A; 5. Journal of Energy Storage; 6. Journal of Membrane Science;
7. Abstracts of papers of the American Chemical Society; 8. Applied Energy;
9. ACS Applied Energy Materials; 10. ACS Applied Materials & Interfaces.

Publication number

(c)

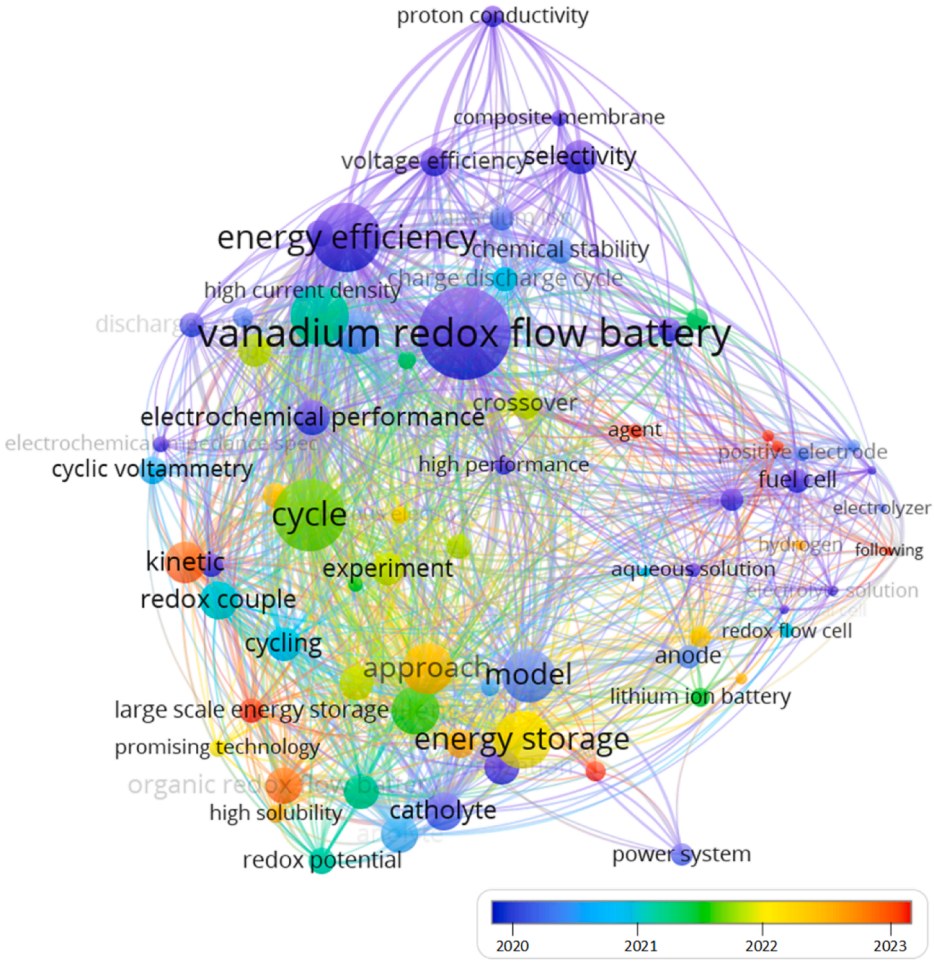

(d)

Fig. 2. (*continued*).

Acta", with 533, 332, and 312 respective publications. The total citation number of 533 papers published in the Journal of Power Sources amounts to 21,481, with an average citation frequency of 40.3.

A scholarly analysis was conducted using VOSviewer software to examine 2298 pieces of literature on RFBs over a period of three years, as shown in Fig. 2**(d)**. The objective of this analysis was to identify keywords that appeared more than 100 times. It was found that the keyword "vanadium redox flow battery" appeared most frequently, indicating its prominence in the field. The analysis also revealed that the vanadium flow battery is currently the fastest-developing RFB with a positive future outlook. Additionally, keywords such as energy storage efficiency and lithium-ion battery were also identified as prominent in the literature.

2.1. Experimental study

Under the assistance of NASA, a number of redox battery stacks were created and examined, and among them, the iron-chromium system flow battery [61] was selected for further development. Various enhancements were made to the battery, including the fabrication of effective carbon electrodes [62,63] and the optimization of temperature, electrolyte, and membrane models to different extents [64]. Nonetheless, the commercial development of the battery has been hampered by factors such as severe ion exchange membrane pollution, low battery capacity density, slow electrode surface reaction, and other unfavorable reasons.

The issue of cross-contamination caused by ion diffusion in ion-exchange membranes in redox flow batteries has been extensively investigated by previous researchers. In 1985, Skylllas-Kazacos [65] proposed a novel all-vanadium flow battery to mitigate the poor reversibility of chromium half-cells and the complexity of developing effective ion-selective membranes. Stability tests indicate that at high temperatures, electrolyte decomposition did not accelerate and that at lower temperatures, there was no crystallization - thus the development of this stable and efficient energy storage battery has broad prospects. Consequently, the development of this stable and efficient energy storage battery holds excellent potential [66]. Following numerous experimental studies, optimization and screening of electrode materials [67–69], membrane [69,70], electrolyte [71–73], electrolyte additives [74], and electrocatalysis [75–77] of all-vanadium flow batteries have been reported. Zhong et al. [78] used two typical graphite felts as electrode materials for all-vanadium redox flow battery (VRFB) and selected different resistivity, pore size, and specific surface area. The results showed that polyacrylonitrile's conductivity is better than rayon's, and polyacrylonitrile's oxidation resistance as an electrode material is stronger. Sharifi et al. [79] focused on studying the water transfer behavior of cation exchange membranes in all-vanadium flow batteries. They researched the impact of vanadium ions on electrolyte density and studied their precipitation behavior in saturated solution under different concentrations and temperatures. Sukkar et al. [80,81] studied the water transfer behavior of cation exchange membranes in VRFB. Their results indicated that the preferred water transfer direction of vanadium electrolyte depends on the state of charge of the electrolyte. They also evaluated the membrane characteristics under different states of charge and found that changes in the state of charge can affect the diffusion rate by altering the ion concentration gradient on the membrane.

Moreover, side reactions occurring at the electrode interface in flow batteries have been found to decrease battery capacity during cycling. Previous studies have investigated these side reactions and their impact on battery performance. In a double-flow system, Sun et al. [82] developed a method to quantitatively measure the hydrogen evolution rate of negative carbon electrodes in VRFBs, revealing that the electrochemical specific surface area of carbon materials significantly impacts the H_2 production rate. Chen et al. [83,84] conducted a potentiostatic method to determine hydrogen precipitation behavior and studied the hydrogen evolution reaction of VRFB on graphite electrodes. Their study showed that hydrogen evolution changes the graphite surface morphology and introduces some defect points on the surface. The electrochemical activity of graphite decreases after hydrogen evolution treatment to the V/V^{2+} electrode. Researchers have also conducted investigations on the influence of electrode surface modification [85,86], battery electrode material [87–89], catalyst [90], electrolyte circulation conditions [91], and other parameters on hydrogen evolution reaction (HER). Under the same conditions, Gahn et al. [92] studied the charge-discharge cycle of different iron-chromium double-flow batteries to measure the effects of cycling on the chromium electrode and film. Zeng et al. [93] proposed a balanced battery design to mitigate the adverse effects of hydrogen evolution on battery capacity in the long-term operation of Fe-Cr redox flow batteries. They utilized the hydrogen produced in the negative electrolyte to reduce excess ferric ions in the positive electrolyte, resulting in a balanced battery system with significantly lower cost. Jayathilake et al. [94] added ascorbic acid to inhibit hydrogen evolution in the electrolyte to reduce the parasitic evolution of hydrogen on the iron electrode. The addition of ascorbic acid regulates pH near the negative surface by buffering, and the increased operating temperature improves iron deposition kinetics relative to the hydrogen evolution reaction, resulting in a net increase in coulomb efficiency (CE). In the single-flow system, Pletcher et al. [95] observed that during the cycle discharge of an all-lead single-flow battery, the lead dioxide on the positive electrode gradually decreased. Wen et al. [96] studied the effect of Pb(II) and H^+ ion concentrations on the electrochemical behavior of all lead single-flow battery electrodes on a composite graphite matrix using cyclic voltammetry (CVA) and constant current charge-discharge methods. Oury et al. [97] examined the oxygen evolution reaction (OER) of α-PbO_2 electrodes in various media in soluble lead-acid flow batteries through electrochemical impedance spectroscopy (EIS) and cyclic voltammetry. Their findings indicated that lead dioxide is more prone to undergo the OER in methane sulfonic acid than in sulfuric acid, suggesting that high-concentration methane sulfonic acid electrolyte exhibits better oxygen extraction performance for lead-acid flow batteries.

The experimental investigation described above has predominantly concentrated on the development and augmentation of electrodes with high efficiency, the formulation of electrolyte composition, and the implementation of flow strategies in flow batteries to enhance their energy density and longevity. Nonetheless, challenges persist, including prolonged cycles, elevated expenses, and a restricted comprehension of the fundamental mechanisms at play, necessitating further attention and resolution.

Table 2
Battery model classification (according to the degree of mechanism involved).

	Empirical model (black box model)	Equivalent circuit model (semi-empirical model)	Electrochemical mechanism model
Advantages	Simple model, accurate results and few parameters	Reflect electrical characteristics, reflect electrochemical law, suitable for practical engineering applications	Less experiment, reflect the internal operation law, conducive to the optimization of battery design
Disadvantages	Large number of experiments, unable to reflect the internal operation rules	Circuit structure is difficult to determine	Complex model, many parameters, computationally heavy, Error exists
Cases	Neural network model, etc	Rint model, Thevenin model, PNGV model, second order RC model, etc	Single particle model, Quasi-2D model, etc

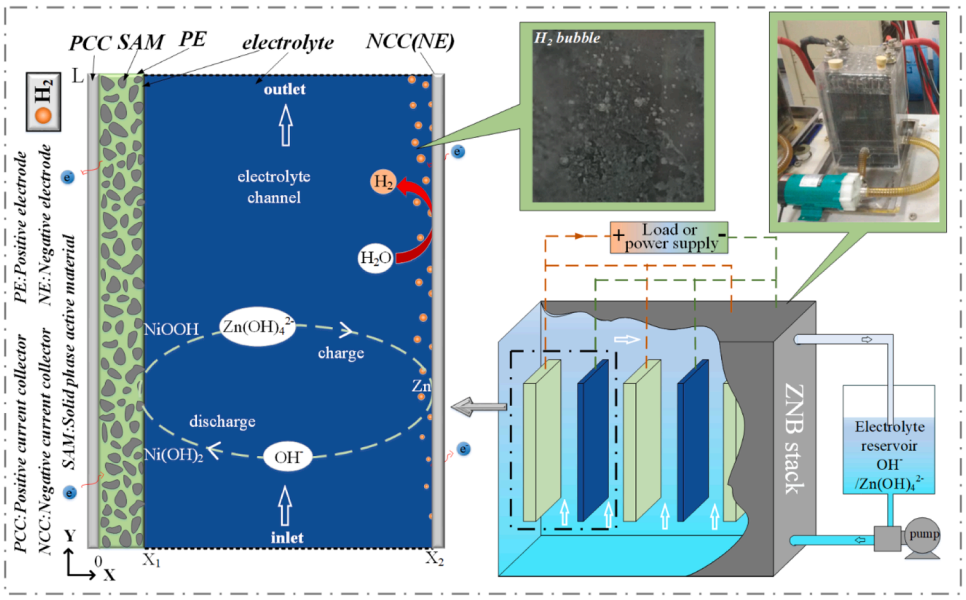

Fig. 3. Structure diagram of ZNB reactor [115].

2.2. Numerical study

Numerical investigations play a crucial role in comprehending the intricate workings of batteries, as relying solely on experimental observations may lead to inconclusive results. Table 2 presents the classification diagram of battery models based on the underlying mechanisms. The empirical model, also known as the black-box model [98], depends on experimental data to establish the mapping connection between output and input. However, it has the disadvantage of not reflecting the internal operations of the battery. On the other hand, the electrochemical mechanism model [99] couples mathematical equations with electrochemical principles to incorporate the internal electrochemical properties of the battery, reflecting its operating law when validated through experiments. The equivalent circuit model [100], also known as the semi-empirical model, is an intermediary between the empirical and electrochemical models. To a certain extent, this model accurately represents the internal electrochemical properties of the battery, and the experimentally derived equivalent circuit, which demonstrates the relationship between voltage and current, provides precise internal parameters of the battery's structure and components.

Currently, there is extensive research on numerical models of VRFBs. Li et al. [101] analyzed the transient behavior of VRFBs from the perspective of chemical reactions and developed an analytical model of the transient characteristics. Their model confirmed that the variation in vanadium ion concentration depends on the chemical reaction and electrolyte flow rate. Similarly, Shah et al. [102] also developed a transient modeling framework for VRFBs, conducting experimental studies on concentration range and electrolyte flow rate and validating their model predictions through experiments. Subsequently, Fetlawi et al. [103] developed a comprehensive non-isothermal model of VRFB with mass, energy, and momentum conservation to describe the transport properties of charge carriers, thermal effects, and the global kinetic model of vanadium-containing reactions. The numerical results demonstrated that operating temperature variation affects battery performance. The variation of electrolyte flow rate and applied current substantially changes the temperature distribution of the charge/discharge characteristics. Conversely, You et al. [104] focused on simulating the migration process of vanadium ions in batteries using mass transfer theory. Their findings indicated that the diffusion rate of vanadium ions is influenced by the concentration gradient between the two tanks and the diffusion coefficient. Ma et al. [105] established a steady-state isothermal three-dimensional dynamic model of VRFB to investigate the impacts of electrolyte velocity distribution on concentration, over-potential, and transfer current density. To prevent thermal precipitation in the electrolyte and overheating of the battery components, Tang et al. [106] included a thermal model based on mass and energy balance in self-discharge for temperature control. Numerical results demonstrated that the model optimized the design and manufacture of batteries. Zheng et al. [107] formulated a comprehensive three-dimensional thermal analysis model to better understand the thermal behavior of VRFB and determine the quasi-static characteristics of temperature and its spatial distribution by analyzing the thermal model. Wang et al. [108] utilized the optimization method based on channel section reconstruction to VRFBs and established a three-dimensional numerical model to study battery performance and mass transfer behavior. They found that the semi-circular channel section exhibited the highest discharge voltage and the lowest charging voltage in VRFB, and the uniformity coefficient of active substances in the passage was 15.4 % higher than that of the triangular passage, thus confirming the feasibility of the semi-circular passage section design.

The serious ramifications of flow batteries have been extensively researched. A 2-D non-isothermal model to investigate the effects of oxygen evolution and bubble formation on VRFBs' battery performance was developed by Shah et al. [109,110]. The multi-phase mixture model was used to describe the transport of gas bubbles through the electrodes [111]. The results showed that the increase of electrolyte flow rate is beneficial to the decrease of oxygen volume in the positive electrode, and charging efficiency for the battery significantly decreased due to bubble precipitation. Furthermore, the electrochemical reaction was explained in detail, and an all-VRFB hydrogen evolution model was established, with numerical results validated through experimental data to prove the impact of the gas release on cell efficiency. In the single-liquid flow system, such as the aluminum-air battery, Wang et al. [112] studied the effect of parasitism on battery performance and evaluated the possibility of hydrogen parasitism evolution improving the total power output. Similarly, Zhou et al. [113] conducted component-level experiments to measure hydrogen evolution and ionic conductivity under different electrolyte concentrations and systematically investigated the impact of hydrogen evolution on Al-air liquid flow batteries. This investigation provided physical insights into understanding the properties of bubbles generated, grown, and removed from electrodes while elucidating the influence of bubbles on electrochemical

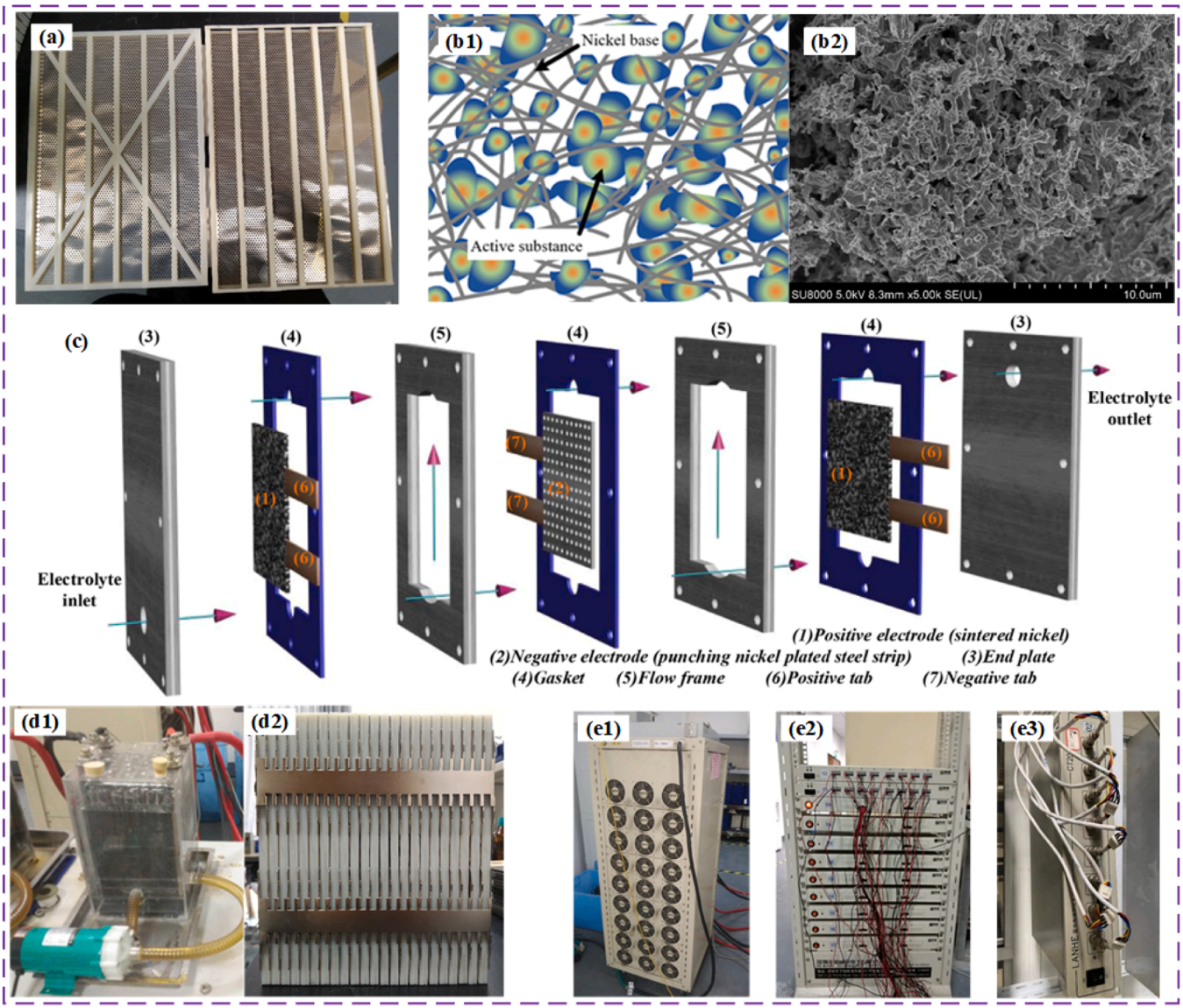

Fig. 4. (a) ZNB negative electrode (punching nickel-plated steel strip); NiO electrode: (b1) porous structure, (b2) SEM schematic diagram; (c) Zinc–Nickel single flow battery testing equipment structure [116]; (d1, d2) Reactor and reactor core of ZNB; Experimental testing instrument: (e1) NTFA detector, (e2) auxiliary test system, (e3) test system.

reactions and the key factors controlling the bubble effect on battery performance. Furthermore, Lao et al. [114] developed a mathematical model to analyze the energy storage application of an integrated system comprising a zinc-air flow battery and a zinc electrolyzer. The model was implemented using MATLAB and verified with experimental results. The study examined the effects of the initial concentration of KOH, electrolyte flow rate, and initial concentration of zincate on battery performance. The model-based analysis aids in comprehending system behavior and enhances the design and operation of the system.

The researchers have conducted thorough numerical investigations and made notable enhancements to the semi-empirical model, enabling a more accurate depiction of the internal workings of batteries. The validity of these advancements has been verified through relevant experimental verifications. As time has passed, the numerical model of the all-vanadium flow battery has progressed from a simplistic, zero-dimensional single battery model to a more sophisticated three-dimensional reactor model. This refined model now incorporates a more precise understanding of various physical fields. Consequently, this development serves as a valuable point of reference for constructing the numerical model of the ZNB in future studies.

3. Basic properties and experimental tests of Zinc–Nickel single flow battery

The development and advancement of numerical mechanism model of the ZNB is founded upon integrating multiple physical field equations within the battery. The selection and refinement of these governing equations rely on the battery's fundamental working principle and basic properties. The construction of numerical models necessitates the comparison and validation of experiments. It is imperative to consider the models' accuracy and computational efficiency to avoid errors. Additionally, the assumptions underlying the various basic equations utilized in the model may introduce certain errors. On the other hand, experimental data under corresponding initial conditions is essential in determining whether the model error is within an acceptable range. As such, validating and enhancing the model's accuracy through experimental tests is paramount. This section provides a brief overview of the basic properties of the ZNB and the pertinent experimental tests conducted for model validation.

3.1. Working principle

The structure diagram of the ZNB reactor is depicted in Fig. 3, comprising the reactor core, electrolyte pump, electrolyte storage tank, load, external circuit system, and electrolyte flow pipeline.

As an illustration of the charging process in the Zinc–Nickel single flow battery, renewable energy or surplus electric energy from the grid acts as the power source, which drives the pump to collect the electrolyte solution, and the solution slowly flows into the channel from the bottom. The electrons obtained on the negative surface are converted into solid zinc, which is deposited on the electrode surface and released into the electrolyte. However, because of the H_2 evolution side reaction, H_2 bubbles tend to precipitate slowly in the electrolyte, while the oxygen precipitates in porous positive electrode through oxidation reaction. Additionally, as the electrolyte flows out of the ZNB reactor via the upper part of the flow channel into the external storage tank, it can re-enter the lower part of the battery, allowing the cyclic reaction to continue. Concerning the discharge process of the ZNB, the reactor functions as the power source, and the operation process is consistent with the charging reaction image. In essence, the hydrogen and oxygen irreversible side reaction is essentially the same reaction. To provide a concrete example within the context of a single battery, the corresponding electrochemical equation can be expressed as follows [116]:

$$\text{Positive}: \quad 2NiOOH + 2H_2O + 2e^- \rightleftarrows 2Ni(OH)_2 + 2OH^- \qquad E_0 = 0.490V \tag{1}$$

$$\text{Negative}: \quad Zn + 4OH^- \rightleftarrows Zn(OH)_4^{2-} + 2e^- \qquad E_0 = -1.285V \tag{2}$$

$$\text{Positivesideeffect}: \quad 4OH^- = O_2\uparrow + H_2O + 4e^- \qquad E_0 = 0.401V \tag{3}$$

$$\text{Negativesidereaction}: \quad 2H_2O + 2e^- = 2OH^- + H_2\uparrow \qquad E_0 = -0.828V \tag{4}$$

3.2. Related material properties

Fig. 4**(a)** illustrates the negative electrode of nickel-plated steel strip (NS), which has been punched for use in the ZNB. Previous experimental studies have employed several materials, including stainless steel, copper, manganese, copper, and nickel-plated steel strip, for comparison.

ZNB performance is considerably influenced by parameters related to the electrolyte, such as ion concentration, tank capacity, flow rate, and the active components in the electrolyte. In this experiment, the electrolyte consists mainly of aqueous solutions of $OH^-$and $Zn(OH)_4^{2-}$, with a small number of additives added to prevent zinc dendrite growth and protect the anode. Fig. 4**(b1)** shows the nickel oxide electrode, where presents the porous structure diagram of the positive electrode, which contains a fibrous nickel substrate and porous nickel supporting the reactive material ($NiOOH/Ni(OH)_2$) of the cell. Fig. 4**(b2)** illustrates the scanning electron microscope image of the active substance, revealing that it is mostly granular or columnar in shape.

During the charging process, NiOOH is produced by oxidation reaction on the surface of ZNB positive electrode. In the active substance, the diffusion coefficient of proton is shown as follows:

$$D_H = D_1\left[SOC + (D_2/D_1)^{1/2}(1 - SOC)\right]^2 \tag{5}$$

where D_1 and D_2 are the diffusion coefficients in proton $Ni(OH)_2$ and NiOOH, respectively.

During the battery charging process, due to oxygen precipitation occurs, the porosity of the positive electrode is gradually reduced. The porosity change of positive electrode is shown as follows:

$$\varepsilon = \varepsilon_0\left(1 - \alpha_{g,O_2}\right) \tag{6}$$

where α_{g,O_2} is the volume fraction of oxygen, and ε_0 is the porosity of the positive electrode without oxygen precipitation.

3.3. Properties of hydrogen and oxygen evolution parasitic reactions

The parasitic reactions of hydrogen and oxygen evolution in the ZNB significantly impact the cycle life and efficiency for batteries. The OER at the battery cathode contributes to the consumption of the active material of the nickel oxide electrode due to the simultaneous precipitation of hydroxide ions into oxygen and alkaline conditions in the electrolyte. Likewise, water is oxidized to produce hydrogen in the hydrogen evolution reaction (HER) while OH^- is produced simultaneously. Similar to oxygen uptake, the hydrogen evolution reaction also affects zinc deposition. Therefore, the electrolyte solution's pH value closely influences the equilibrium potential between the two gas electrodes.

(1) According to Nernst equation, the equation of equilibrium potential of hydrogen evolution reaction is:

$$E_{e,H_2} = E_{O,H_2} + \frac{RT}{F}\ln\frac{\alpha_{H^+}}{p_{H_2}^{1/2}} \tag{7}$$

where α is the activity that is determined by the chemical properties of the substance. In addition, gas is regarded as an ideal gas, and its activity is represented by the gas partial pressure ratio. The activity takes the form of $\alpha = p/p_0$, where$p$and p_0 are the pressure and the partial pressure in the standard state (1atm), in respective.

The relationship between proton activity and pH value in solution takes the form of:

$$PH = -\lg\alpha_{H^+} = -\frac{1}{2.303}\ln\alpha_{H^+} \tag{8}$$

The equilibrium potential of hydrogen evolution reaction is:

$$E_{e,H_2} = E_0 - \frac{2.303RT}{F}\ln\left(PH + \frac{1}{2}\lg p_{H_2}\right) \tag{9}$$

(1) The expression of equilibrium potential of oxygen evolution reaction (OER) is:

$$E_{e,H_2} = E_{o,O_2} + \frac{RT}{4F}\ln\frac{p_{O_2}}{\alpha_{OH^-}^4} \tag{10}$$

The relationship between OH^- activity and pH value of solution yields:

$$PH = -\lg\alpha_{OH^-} + 14 \tag{11}$$

The equilibrium potential of hydrogen evolution reaction is:

$$E_{e,H_2} = E_{0,O_2} + \frac{RT}{4F}\ln\left(\frac{1}{2}\lg p_{O_2} - 4PH + 56\right) \tag{12}$$

The Bulter-Volmer equation is exploited to describe the reaction rate of hydrogen/oxygen evolution, and the influencing mechanism between the main/side reaction is revealed. It expressed by the following equation:

$$j = j_0^0\left(\frac{c_R^*}{c_R^{0*}}e^{\beta nF\eta/(RT)} - \frac{c_P^*}{c_P^{0*}}e^{-(1-\beta)nF\eta/(RT)}\right) \tag{13}$$

where η denotes the activation over-potential, and the surface concentrations of reactants and products are expressed as c_R^* and c_P^*. n represents the number of electrons transferred in the electrochemical reaction, and the current density in the standard reference state is expressed as j_0^0. As the hydrogen evolution and oxygen evolution side

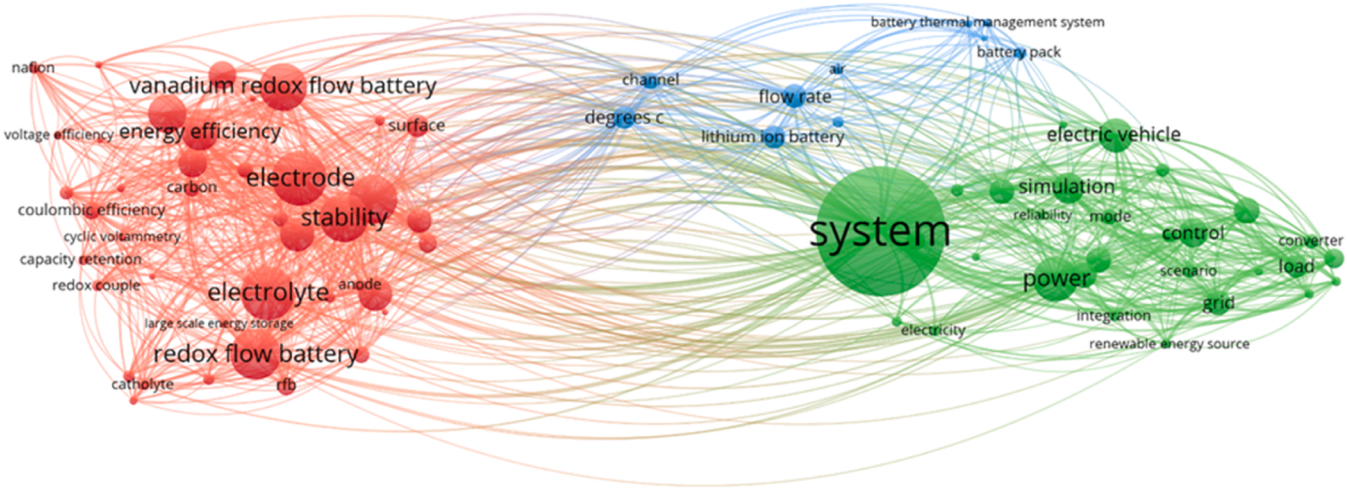

(a)

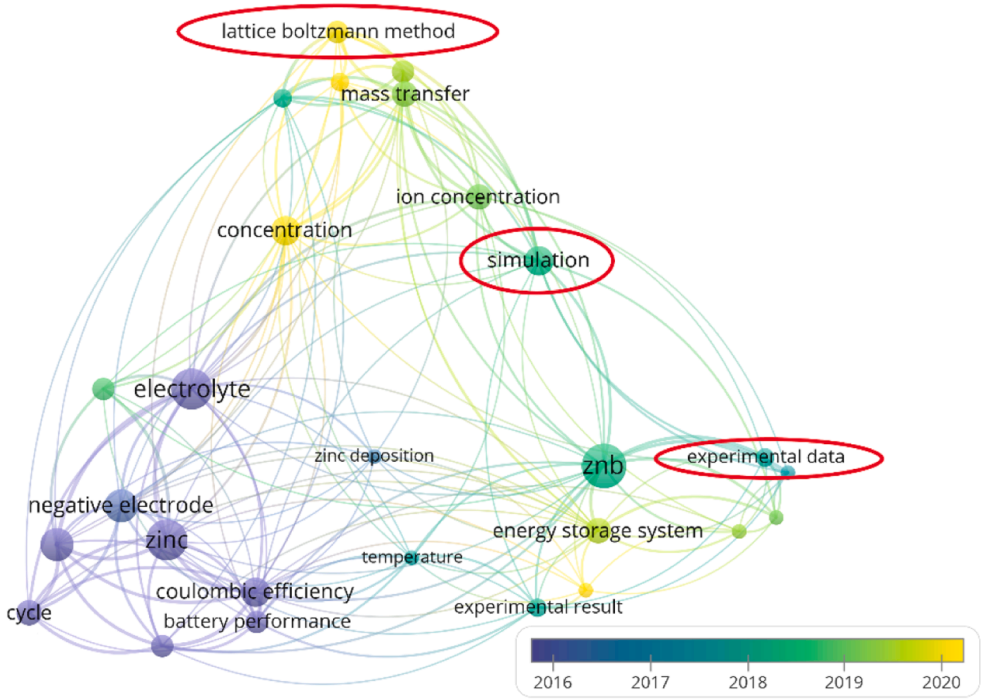

(b)

Fig. 5. Keyword Search of ZNB published in recent 5 years (more than 25 times); (b) Research retrieval of ZNB by our research group in recent 5 years.

reactions are highly irreversible, transfer coefficient is $\beta(0<\beta<1)$, which represents how the change of the reaction interface potential changes the size of the activation energy barrier of the forward reaction and the reverse reaction. Therefore, the second term in the right parenthesis of Eq. (13) is usually ignored.

The high irreversibility of HER and OER results in decreased efficiency of the ZNB during the charge/discharge process caused by the depletion of a certain current density. The coulomb efficiency of the battery is used to assess the impact of the side reaction on the performance of the ZNB, and the relevant formula is expressed by:

$$CE = \frac{\int_0^{t_d} I_d dt}{\int_0^{t_c} I_c dt} \tag{14}$$

where CE is the Coulomb efficiency, I denotes the current density. The lower corner script d represents the charging process, and the lower corner script t represents the discharge process.

3.4. Battery test

3.4.1. Experimental subjects

(1) Plate-groove test kit

For experimental purposes, the plate-groove Zinc–Nickel single flow test battery is depicted in Fig. 4**(c)**. The test battery includes two sets of electrodes, two sintered nickel positive electrodes, a stamped nickel-

Table 3
Important advances in experimental and numerical simulations of ZNB.

Refs	Research means	Research objective	Main conclusions
[117]	experiment	Battery structure and corresponding theoretical construction	1 Zinc–Nickel single flow battery was proposed; 2 The average coulomb efficiency is 96 % and the energy efficiency is 86 %.
[54]	experiment	Zinc deposition phenomenon	1 In the flowing electrolyte, no zinc dendrites occur on the surface of cadmium substrate; 2 The coulomb efficiency and voltage efficiency of the battery reached 98 and 88%, respectively.
[118]	experiment	Electrochemical behavior of zinc deposition/dissolution	Nickel-plated punch steel strip has stable performance and high hydrogen evolution over-potential.
[120]	experiment	Zinc dendrite growth	Pb (II) and TBAB have synergistic effects on the growth of spongy zinc dendrites.
[121]	experiment	Sharp decline in performance (rapid charge and discharge)	1 A cell structure of serpentine flow field was designed; 2 The efficiency of the battery increased by 10.3 % at 80 mA cm^{-2}.
[123]	experiment	Zinc deposition and dissolution	1 NF has a good effect on zinc deposition and dissolution; 2 After 200 cycles, high coulombic efficiency (97.3 %) and energy efficiency (80.1 %) were obtained.
[125]	experiment	Potential distribution and side effects	1 The coulomb efficiency increases first and then decreases with the increase of current density; 2 The increase of current density results in the formation of zinc dendrites.
[127]	experiment	Hydrogen evolution reaction	1 The hydrogen evolution reaction begins near the limiting current density of zinc deposition; 2 Hydrogen bubbles enhance the mass transfer of zincate ions to the electrode surface.
[128]	experiment	Composite cathode structure	1 For 500 cycles, the average coulomb efficiency and energy efficiency were 99.2 % and 84.2 %, respectively; 2 No zinc dendrite deposition in nickel-oxygen hydroxide composite electrode.
[131]	Numerical simulation	Three-dimensional steady-state model (Electrode current density and internal ion concentration)	The model can well simulate the charge-discharge characteristics of ZNB under constant current condition.
[132, 133]	Numerical simulation	Equivalent circuit model (Charging and discharging power and charging state)	1 The model charging and discharging voltage error ranges from 0 to 3.85 %; 2 The flow optimization effect of genetic algorithm is better under the condition of charging and discharging power and charging state change.
[134, 135]	Numerical simulation	Two-dimensional transient model (Concentration, flow rate, and applied current density)	1 Increasing the concentration of hydroxide ion increases the discharge voltage; 2 The increase of flow rate facilitates the consumption of reactants and accelerates mass transfer; 3 The effect of flow rate on battery discharge voltage is small and limited.
[116]	Numerical simulation	Three-dimensional transient model (Hydrogen evolution reaction)	1 Reducing the applied current density, ambient temperature and increasing the flow rate of electrolyte can inhibit the hydrogen evolution reaction; 2 The existence of side reaction makes the activation polarization of positive electrode more obvious.
[136]	Numerical simulation	Three-dimensional transient model (Global polarization distribution)	1 Porous nickel foam (NFs) reduces overall polarization compared to nickel foam as a negative electrode; 2 The influences of nickel foam thickness, nickel foam porosity and inlet electrolyte flow rate on polarization were optimized by RSM.
[145, 146]	Numerical simulation (Void scale)	Porous electrode positive structure	1 The proton concentration has obvious influence on the reaction rate and current density; 2 The concentration of hydroxide has great influence on the over-potential.
[147]	Numerical simulation (Void scale)	Evolution of zinc dendrites, spatial and temporal distribution of ions/electrons	1 The adjustment of anisotropy intensity can reduce the formation of dendrites; 2 The ionic diffusion rate increases with the increase of electrolyte flow velocity.
[148]	Numerical simulation (Void scale)	Flow mass transfer of porous electrodes	1 Under different pore structures, the decrease of porosity and particle size increases the diffusion rate of electrolyte ions; 2 The increase of electrode thickness affects the diffusion of OH- ions and intensifies the concentration polarization.

plated steel negative electrode, a sealing ring to prevent electrolyte leakage, and a flow frame. During the test process, the electrolyte enters the bottom of the battery, undergoes an electrochemical reaction with the electrode, and flows out from the upper part of the battery. Notably, this test tool has a flexible and convenient structure, allowing easy disassembly and assembly. It can accommodate electrodes with a maximum width of 59 mm and a maximum height of 29 mm. The primary focus of its application is in single battery experimental research studies.

(1) ZNB reactor

A ZNB reactor structure is presented for battery reactor performance testing is shown in Figs. 4**(d1)** and **(d2)**. The second-generation ZNB, created by Zhejiang Yuyuan Energy Storage Co., LTD., comprises 240mm × 150mm × 0.32mm sintered nickel with 0.44 porosity and 240mm × 150mm × 0.08mm nickel-plated steel strip, delivering a 300 Ah capacity consisting of 23 batteries in parallel. The electrolyte tank has a volume of 5.76 L, and the width of the electrolyte channel between positive/negative electrodes is 3.8 mm.

3.4.2. *Test equipment and test methods*

In Fig. 4**(e1)**, the 5V200A-NTFA battery tester developed by New Will Electronics Co., LTD., Shenzhen, is presented as a device for measuring battery voltage, temperature, constant power charging, and pulse work step parameters, supported by the BTS7.5.X battery detection software system. Fig. 4**(e2)** displays the battery-assisted test system for examining a single battery's temperature or voltage data, controlling and resetting sub-channel mapping. In Fig. 4**(e3)**, the Blue Battery Test System No. CT2001A can be observed, which is utilized for multi-parameter and complex charging and discharging processes, including constant voltage charging and discharging and static positions, and can be programmed using UDFs. Using the constant current charging and discharging procedure, voltage data of the experimental battery during the charging/discharging process is obtained and then compared with numerical simulation charging/discharging processes. Such analysis allows for evaluating the accuracy and reliability of the numerical model and numerical process.

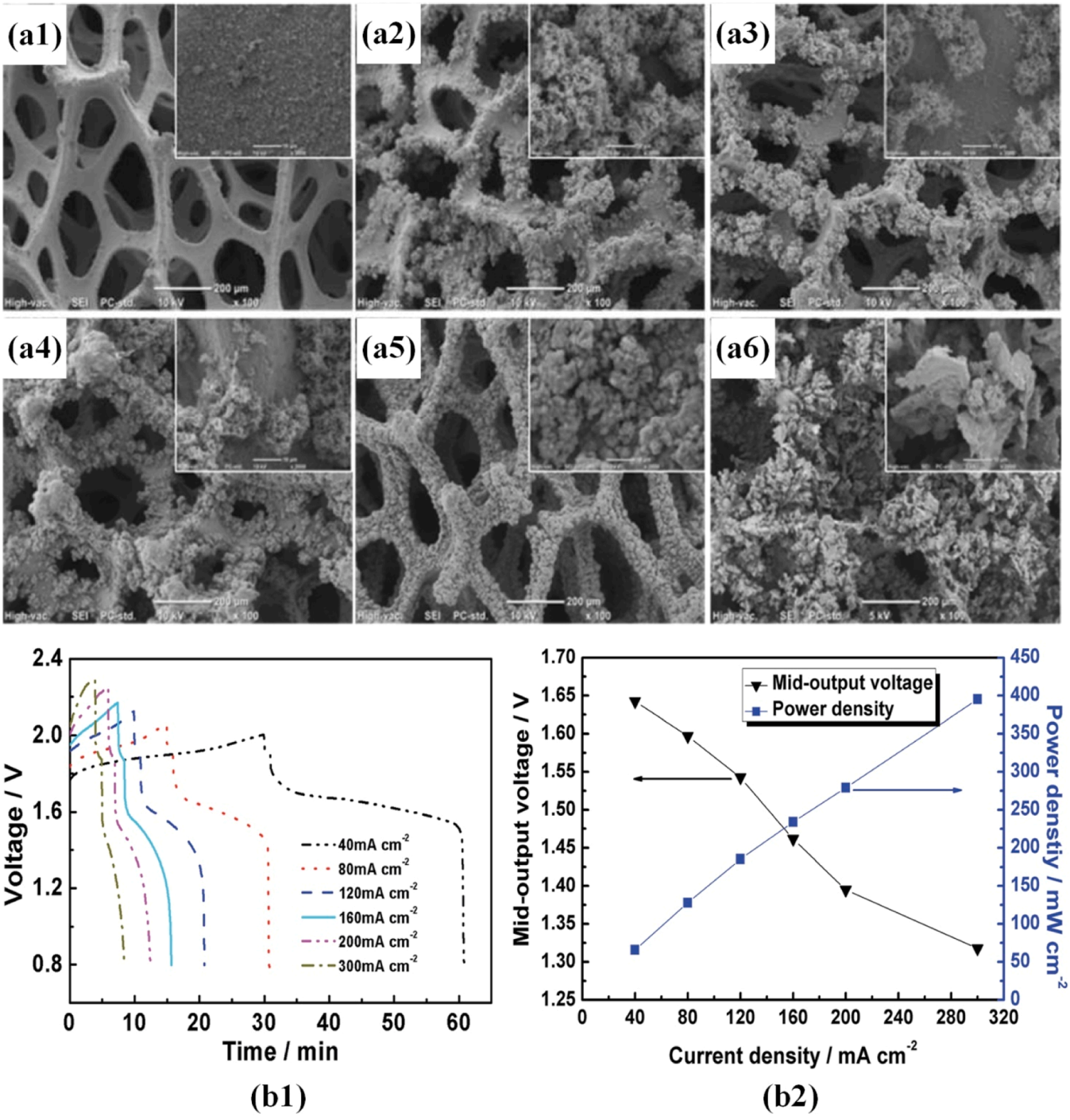

Fig. 6. Morphologies of deposited zinc on negative electrode at various current densities: (a1) 40 mA cm^{-2}, (a2) 80 mA cm^{-2}, (a3) 120 mA cm^{-2}, (a4) 160 mA cm^{-2}, (a5) 200 mA cm^{-2}, (a6) 300 mA cm^{-2}. At different current densities (40 mA cm^{-2} to 300 mA cm^{-2}): (b1) Charge/discharge voltage curves; (b2) Mid-output voltage and power density [125].

4. Research status of Zinc–Nickel single flow battery

In 2007, Cheng et al. [117] first proposed the single-flow Zn/NiOOH battery, a novel redox flow battery. Experimental results indicated that the battery demonstrated excellent performance, with an average coulomb efficiency and energy efficiency of 96 % and 86 %, respectively, during 1000 cycles. Over more than ten years, this new flow battery has progressed into the industrial demonstration stage. Subsequently, a keyword search of ZNB published in the last 5 years was conducted. Utilizing visual literature analysis software VOSviewer, over 25 keywords were examined, and the outcomes are presented in Fig. 5 **(a)**. The study of battery systems has remained the primary research focus for ZNB. Moreover, there has been a particular emphasis on redox flow battery, vanadium flow battery, and electrode investigations, employing numerical simulation and experimental research as the principal research methods [57].

The research trajectory concerning ZNB in the preceding five years is illustrated in Fig. 5**(b)**. Visual retrieval reveals that since 2016, research on ZNB has primarily concentrated on electrode preparation, mass transfer process, and battery system experimentation. Notably, there has

been a gradual upsurge in research employing the Lattice Boltzmann Method (LBM) to scrutinize the internal workings of ZNB. It is worth emphasizing the profound significance of multi-physical field and multi-scale numerical research in the context of the ZNB system (Table 3).

4.1. Experimental study

The electrolytes in ZNB, specifically those in the positive and negative electrodes, consist of highly concentrated ZnO in KOH aqueous solution. The negative electrode comprises an inert metal, such as nickel foil, while the positive electrode is made of NiO. Because of its membraneless structure, its cost is lower. However, notable issues such as significant polarization loss, low energy density, and dendrite growth can impact battery capacity, leading to reduced efficiency [117,118]. To address these challenges, extensive research has been conducted, aiming to enhance the energy density of the battery and minimize energy loss during cyclic charging and discharging, thereby promoting the overall development of ZNB technology.

Zhang et al. [54] studied zinc deposition in basic zincate solution in the ZNB. They observed that the cadmium substrate performed exceptionally well in the flow electrolyte, as there was no evidence of zinc dendrite formation on its surface. The battery achieved a coulomb efficiency of 98 % and a voltage efficiency of 88 %. Cheng et al. [118] evaluated the effects of nickel foil and nickel-plated perforated steel strips as substrate electrodes on the electrochemical behavior of zinc deposition/dissolution in a flowing electrolyte. Nickel-plated perforated steel strips exhibited excellent stability and high hydrogen evolution over-potential, rendering it a superior electrode choice. By studying the cycling stability of nickel oxide electrodes with zinc ions in ZNB electrolyte, Cheng et al. [119] found that zinc reduced the charging voltage of electrolyte to a certain extent, leading to significant improvements in nickel oxide electrode cycling performance while curbing variations in the constant current charging curve with number of cycles. Incorporating zinc ions into the lattice structure of nickel metal hydride oxides to form composite materials proved a potential solution for improving battery cycle performance. Wen et al. [120] examined the performance of lead ion and tetrabutylammonium bromide (TBAB) on ZNB using various methods. Their results demonstrated that the synergistic effect of Pb(II) and TBAB inhibited the growth of spongy zinc dendrites, effectively improving the battery's anode charging performance. Cheng et al. [121,122] observed a sharp decline in battery performance during rapid charge and discharge, prompting the development of a new battery structure with a serpentine flow field. This architecture prevented significant efficiency reductions over 70 cycles of charging and discharging. Compared to conventional battery structure, the energy efficiency of the battery at 80 mA cm^{-2} increased by 10.3 %, significantly improving efficiency. A new type of negative electrode with a good mass transfer structure and large reaction area is designed to promote the parasitic reaction of negative electrode, representing an effective means of improving the cycling stability of ZNBs. Then, for the first time in ZNBs, a three-dimensional porous electrode, nickel foams (NFs), was introduced [123]. Results indicated that NFs exhibited good effects on zinc deposition and dissolution. When zinc deposition on NFs at 20 mA cm^{-2}, conducted 200 times at 80 mA cm^{-2} with NFs as negative electrode, and obtained higher coulombic efficiency (97.3 %) and energy efficiency (80.1 %).

Cheng et al. [124] conducted experiments to examine the adaptability of ZNB to temperature and the impact of temperature and polarization distribution trends on battery performance. The findings revealed that ZNB operates within a temperature range of 0 °C~ 40 °C, with energy rates ranging from 53 % ~ 79.1 %. Positive polarization significantly surpassed negative polarization, with temperature exerting a more pronounced impact on the positive electrode charge over-potential. Additionally, Cheng et al. [125] studied the potential distribution of batteries and the influence of side reactions at a current density of 300 mA/cm^2. The results indicated that the presence of side effects and uneven potential distribution initially increased the Coulombic efficiency but then decreased with increasing current density. Fig. 6**(a)** shows the influence of different current densities on the zinc deposition morphology on the negative electrode. As the current density increases from 40 mA cm^{-2} to 300 mA cm^{-2}, the zinc deposition morphology in Fig. 6**(a1)** is smooth, that in Fig. 6**(a2-a5)** is spongy, and that in Fig. 6**(a6)** is dendrite. Therefore, with high current density, the deposition of zinc dendrites can be reduced by increasing the mass transfer of active substances. Fig. 6**(b1)** displays (b1) charge/discharge voltage curve, and Fig. 6**(b2)** moderate output voltage and power density changes under different current densities (40 mA cm^{-2} to 300 mA cm^{-2}).

Additionally, Ito et al. [126] evaluated the influence of flowing electrolytes on gas precipitation and discovered that the precipitation of hydrogen and oxygen could be inhibited through electrolyte circulation. In addition, the coulomb efficiency under flow condition was higher than that under non-flow condition, and in deep discharge, more hydrogen was generated under flow condition than non-flow condition. Dundalek et al. [127] conducted an experimental investigation to examine the complex effect of hydrogen evolution reaction (HER) on the deposition of zinc electrodeposition. Results revealed that the HER initiates near the limit current density of zinc deposition, and then the current efficiency is reduced. Additionally, the rise of hydrogen bubbles enhances the mass transport of zincate ions to the electrode surface, somewhat compensating for the decrease in current efficiency. Wang et al. [128] proposed a novel ZNB with a composite cathode (Ni$(OH)_2$-O_2) and an improved electrolyte, KOH-$K_2[Zn(OH)_4]$. Results revealed that on the first 500 cycles, the average coulomb and energy efficiency were 99.2 % and 84.2 %, respectively. Moreover, they observed the absence of zinc dendrite deposition at the end of discharge and demonstrated significant performance improvement by applying the nickel-oxygen hydroxide composite electrode in the ZNB.

The outcomes of these experiments demonstrated the positive impact of optimization on the lifespan extension and efficiency enhancement of ZNB technology. Nevertheless, comprehensively analyzing the reaction mechanism and electrochemical phenomena occurring within the battery presents difficulties due to the considerable expenses of conducting such experiments. As a result, numerical investigations of ZNB have been progressively undertaken to explore the fundamental principles governing the internal battery mechanism and the alterations in associated parameters.

4.2. Numerical study

Currently, numerical simulation of ZNB is in its developmental stage, and it holds great potential for providing a deeper understanding of the internal mechanism and reaction laws of ZNB. Its development is crucial for reducing polarization loss and increasing ZNB energy density.

Liu et al. [129] were pioneers in proposing the internal mass transfer mechanism of ZNB and a semi-empirical model of the electrochemical reaction. Based on this model, to better comprehend the electrochemical performance of ZNB, Xiao et al. [130,131] established a 3-D steady-state model of ZNB, considering reaction mass, momentum, charge reactions, and focused on the ZNB electrode current density and internal ion concentration distribution. They also simulated the charge-discharge characteristics of ZNB through electrochemical and mechanical models. The equivalent circuit model of a 300Ah ZNB was also established [132,133]. Exponential function fitting and higher order polynomial fitting were used to analyze the model parameters. And the parameter formula obtained by fitting can calculate the battery parameters effectively. Recently, a simulation model considering flow rate, self-discharge, and pump power loss has been established, and experimental comparison suggests that the error range of charge-discharge voltage is between 0 and 3.85 %. The researchers utilized genetic algorithms and various flow factors' theoretical minimum flow times to optimize the variable electrolyte flow during dynamic charging states. In

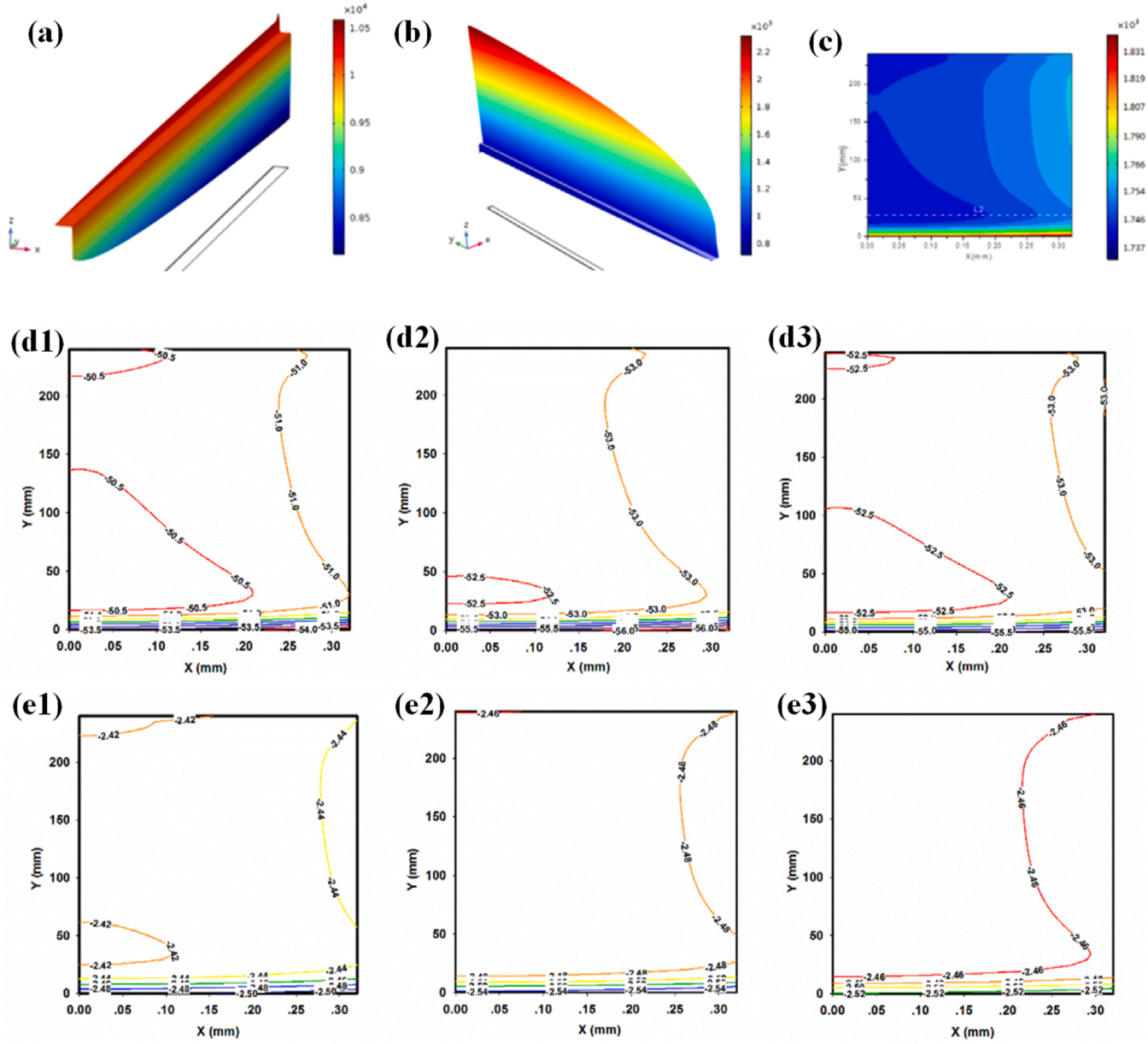

Fig. 7. At 50% SOC for applied current density of 300 mol/m^3, the distribution of (a) OH^-, (b) $Zn(OH)_4^{2-}$ and (c) proton concentration. Distribution of (d) over-potential and (e) transfer current density for (1) OH^- concentration of 9000 mol/m^3, the $Zn(OH)_4^{2-}$ concentration of 300 mol/m^3, (2) OH^- concentration of 11,000 mol/m^3, and the $Zn(OH)_4^{2-}$ concentration of 300 mol/m^3 and (3) OH^- concentration of 11,000 mol/ m^3 and $Zn(OH)_4^{2-}$ concentration of 500 mol/ m^3 [135].

practical engineering, genetic algorithms have demonstrated superior flow optimization effects under changing charging and discharging power and charging states.

In order to obtain a comprehensive understanding of the internal mass transfer mechanism and electrochemical reactions of ZNB, it is imperative to construct a battery model that incorporates multi-physical field coupling. While effective circuit and semi-empirical mechanism models of ZNB offer simplified equations and straightforward solutions, their applicability is restricted and relies heavily on empirical formulas derived from experimental data. As a result, their practical utility is limited.

The current research focus is on the multi-physical field coupling model of ZNB. Yao et al. [134,135] established a 2-D transient model of ZNB, comprehensively considering the reaction mass, the positive and negative electrode flows and chemical reactions between electrode electrolytes. Through experiments, they demonstrated the accuracy of the numerical model and investigated the impact of parameters such as applied current density, flow rate, and concentration on ZNB performance. It had been observed that an increase in hydroxide ion concentration leads to a higher discharge voltage. In contrast, an increase in flow rate promoted reactant consumption and accelerates mass transfer, but had a minimal and limited effect on discharge voltage. Fig. 7 displays the distribution of (a)OH^-, (b)$Zn(OH)_4^{2-}$, and (c) proton concentration at 50 % state of charge (SOC) for an applied current density of 300 mol/m3, as well as the distribution of (d) over-potential and (e) transfer current density for (1) OH^-concentration of 9000 mol/m3 of $Zn(OH)_4^{2-}$, concentration of 300 mol/m^3, (2) OH^-concentration of 11, 000 mol/m^3 of $Zn(OH)_4^{2-}$, concentration of 300 mol/m^3, and (3) OH^-concentration of 11,000 mol/ m3 of $Zn(OH)_4^{2-}$ and concentration of 500 mol/ m^3 of $Zn(OH)_4^{2-}$.

Zhou et al. [116] developed a 3-D transient model of ZNB,

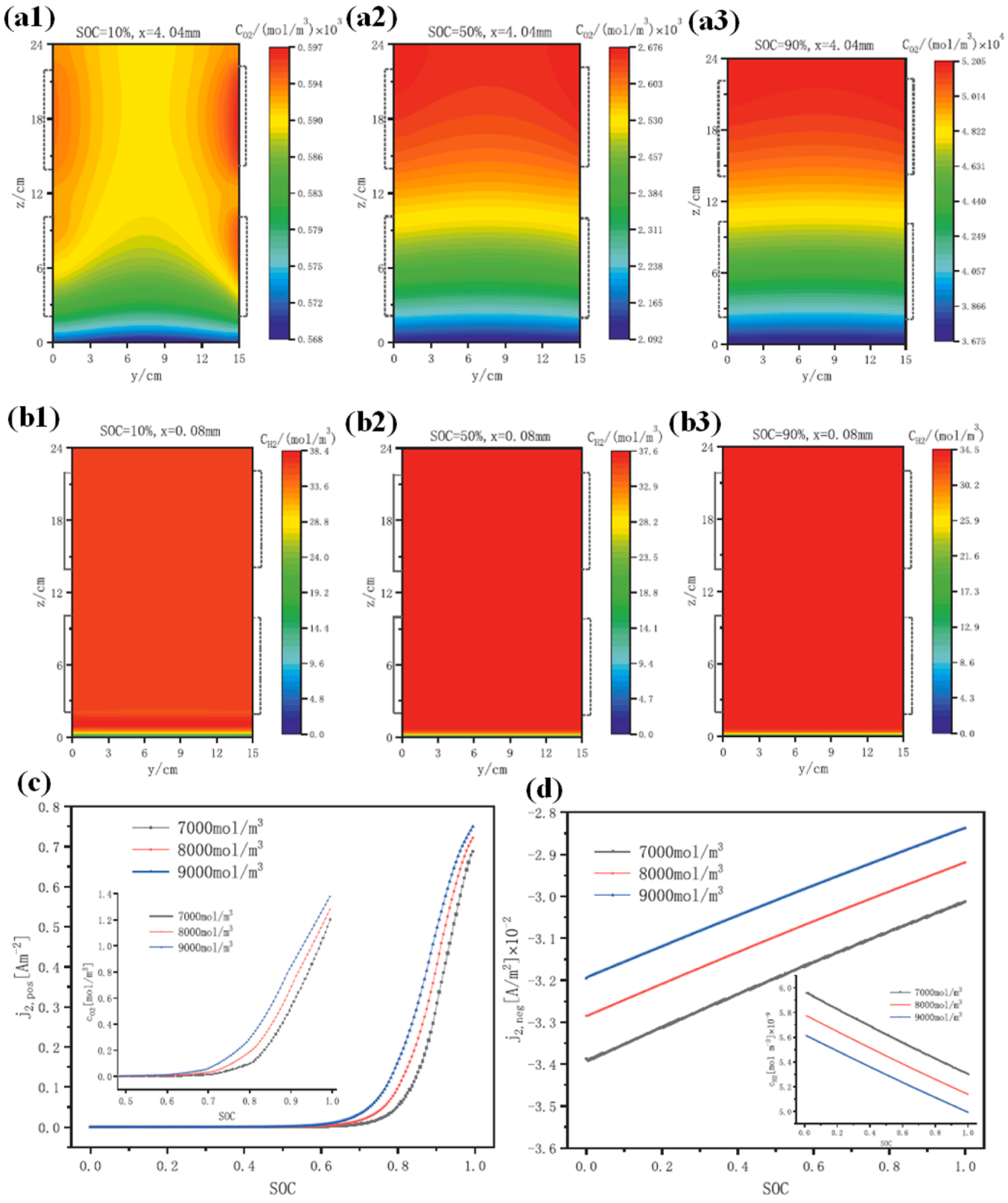

Fig. 8. Under different SOC conditions, the concentration distribution of (a1, a2, a3) oxygen on the middle section of the positive porous electrode layer and (b1, b2, b3) hydrogen on the surface of the negative electrode. At different initial hydroxide ion concentrations, (c) the exchange current density and oxygen concentration of oxygen evolution reaction, and (d) the change of exchange current density and hydrogen concentration of hydrogen evolution reaction with SOC [56].

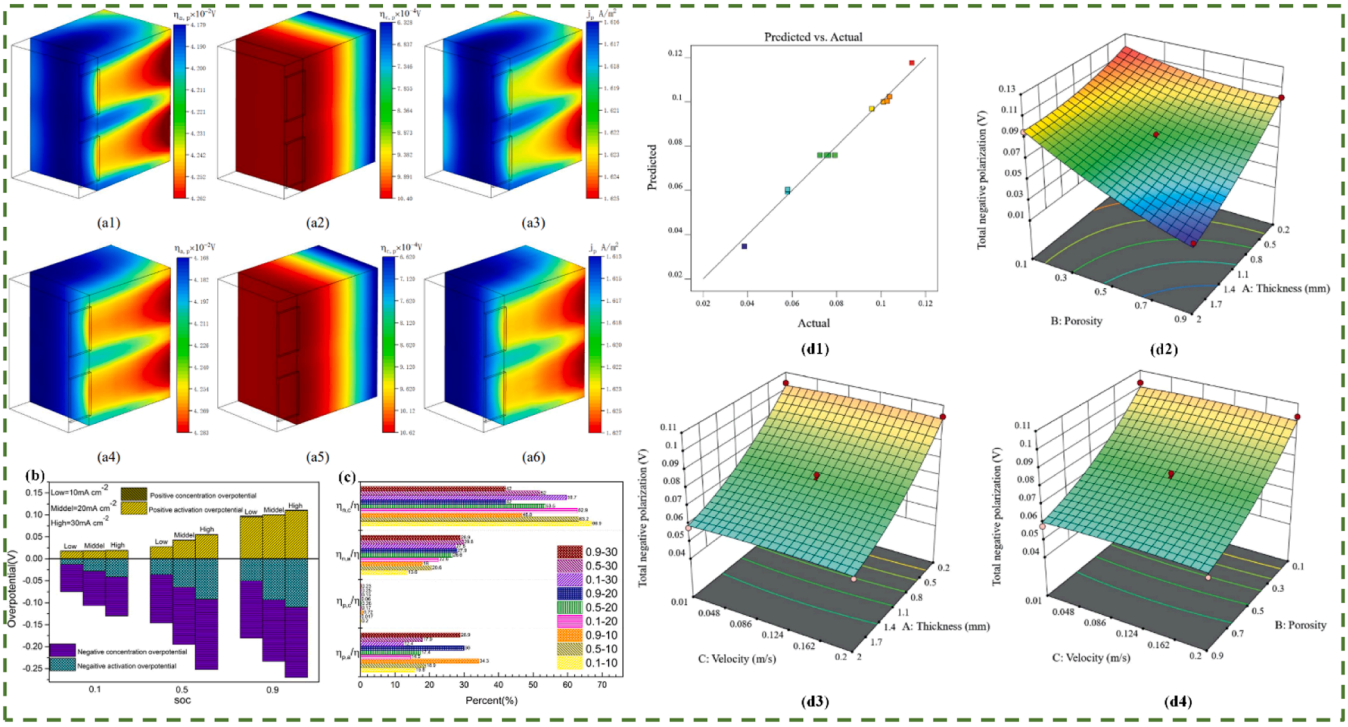

Fig. 9. NS as negative electrode: (a1) positive electrode activation over-potential; (a2) positive electrode concentration over-potential; (a3) positive electrode local density. NF as negative electrode: (a4) positive electrode activation over-potential; (a5) positive electrode concentration over-potential; (a6) positive electrode local density. Over-potential of positive and negative electrodes under different SOC and current density: (b) over-potential distribution; (c) the ratio of positive and negative over-potential to total over-potential [136]. RSM of total negative over-potential: (d1) predicted value vs. actual value of numerical model; (d2; d3; d4) effect of different parameters on the total negative over-potential [137].

considering side reactions. The research revealed that HER inhibition could be achieved by lowering applied current density and temperature and increasing the electrolyte flow rate. The existence of side reactions caused strong positive polarization. Under different SOC conditions, the concentration distribution of oxygen in the middle part of the positive electrode and hydrogen on the surface of the negative electrode, as well as the change of exchange current density and oxygen concentration of hydrogen evolution reaction with SOC, are shown in Fig. 8. Subsequently, based on the three-dimensional transient model of ZNB, Zhou et al. [56] have further investigated the impact of tab design on current density, ion concentration, over-potential, and local state of charge distribution in the ZNB, based on their three-dimensional transient model. The results indicate that increasing tab length and number is crucial for enhancing ion concentration distribution and reducing depressed-pressure loss. Conversely, tab width and position have been found to have minimal influence on voltage loss and ion concentration distribution.

Yao et al. [136] first analyzed the positive/negative electrodes and overall battery polarization, based on the 3-D transient model of ZNB. The study compared the benefits of using porous nickel foams (NFs) instead of NS as the negative electrode. It summarized the optimal thickness and porosity of NFs under various current densities and electrolyte flow rates. Fig. 9 displays NS and NF as ZNB negative electrode: (a1, a4) positive electrode activated over-potential; (a2, a5) positive concentration over-potential; (a3, a6) local density of positive electrode; Positive and negative over-potential at different SOC and current densities: (b) over-potential distribution; (c) Ratio of positive and negative over-potential to total over-potential.

Based on the three-dimensional transient polarization model of ZNB, Huang et al. [137] introduced the optimization method (response surface method, RSM) to study the polarization process. The thickness, porosity of NFs, and flow rate of the inlet electrolyte were selected as variables to investigate the effects of different parameters on the polarization of the negative electrode. The findings of the study, as illustrated in Fig. 9**(d)**, revealed several important insights: (d1) a comparison between the predicted value and actual value of the numerical model; (d2, d3, d4) the influence of different parameters on total negative over-potential. The results indicated that the thickness and porosity of NFs significantly affected the negative concentration polarization and negative activation polarization of ZNB. However, they had a negligible impact on the inlet electrolyte flow rate.

Building upon previous research, a 3-D transient model of ZNB, which considers side reactions, has been successfully established, providing a foundation for future studies on side reactions and cyclic charge-discharge in battery reactors. The existence of side reactions leads to a decrease in the life and capacity of the Zinc–Nickel single flow battery. A mechanism research model was proposed to further investigate the influence of side reactions, which holds significant implications for side reaction studies. Yao et al. [138] proposed a 2-D simulation model to examine the dynamic characteristics of self-discharge under no-load and continuous electrolyte flow conditions. The results revealed that negative side reactions predominantly influence the self-discharge effect, affecting the battery's potential during the initial stage of self-discharge and impeding the rise of battery voltage during the later stage of charging. Adjusting the current density can enhance the battery's coulomb efficiency. Vidts et al. [139] proposed a mathematical model of a sealed nickel-cadmium battery, which includes proton diffusion and ohmic drop of the active substance in the nickel electrode. The calculation results demonstrated that the discharge voltage of the battery is primarily affected by nickel reaction kinetics, and proton diffusion becomes crucial at the end of discharge. Subsequently, Vidts et al. [140,141] constructed a mathematical model of nickel-metal hydride battery, aiming to predict the distribution of electrolyte, hydrogen and oxygen concentrations, hydrogen and oxygen pressures, potential, current density, electrochemical reaction rate, and charge state within the battery. The general governing equations of porous electrodes with

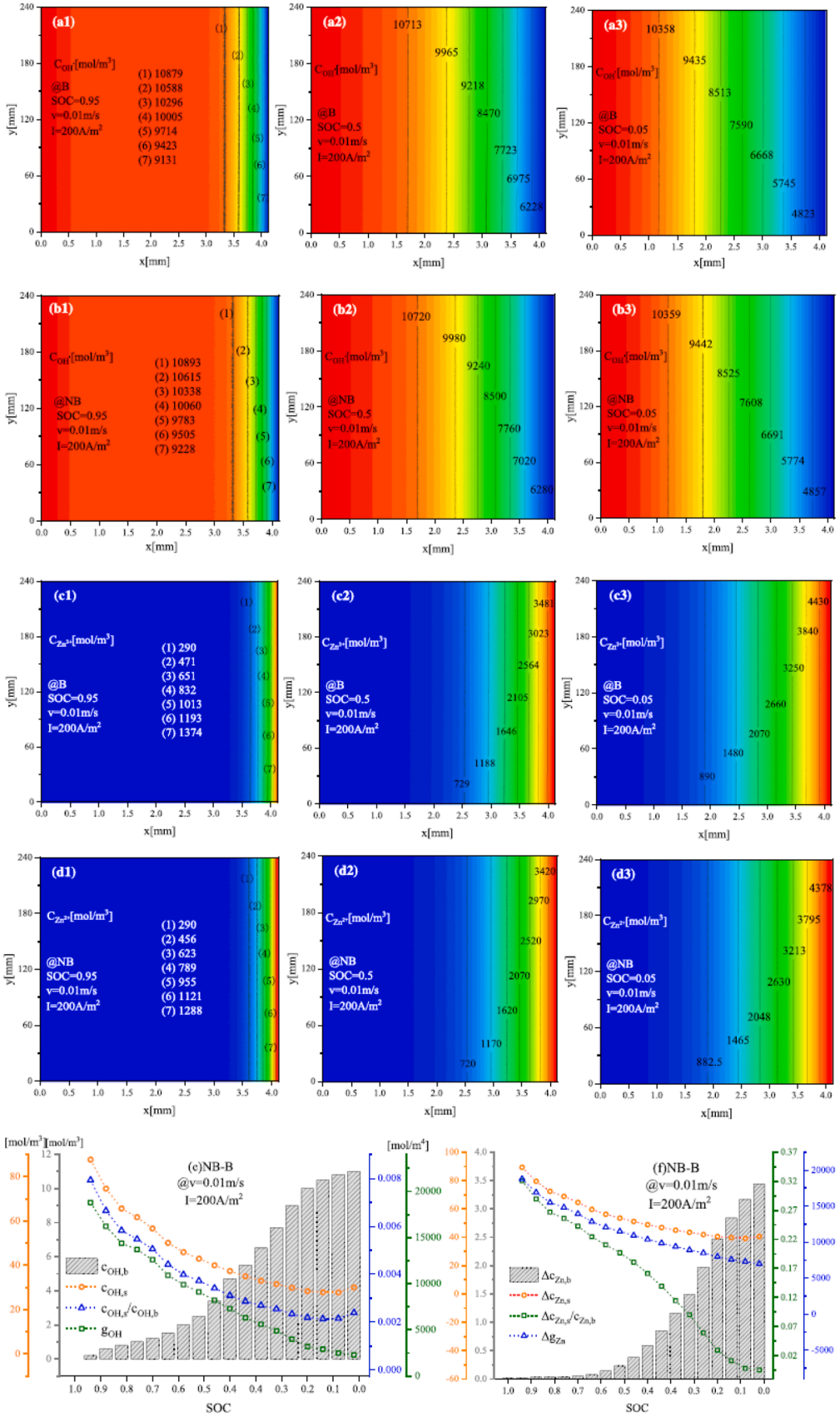

Fig. 10. Under the conditions of (a, c) considering bubble flow and (b, d) not considering bubble flow, the distribution of (a, b) OH^-, (c, d) $Zn(OH)_4^{2-}$ concentration under different SOC conditions; (e) OH^- related parameters varies of SOC with bubble flow and without bubble flow; (f) $Zn(OH)_4^{2-}$ related parameters varies of SOC with bubble flow and without bubble flow [115].

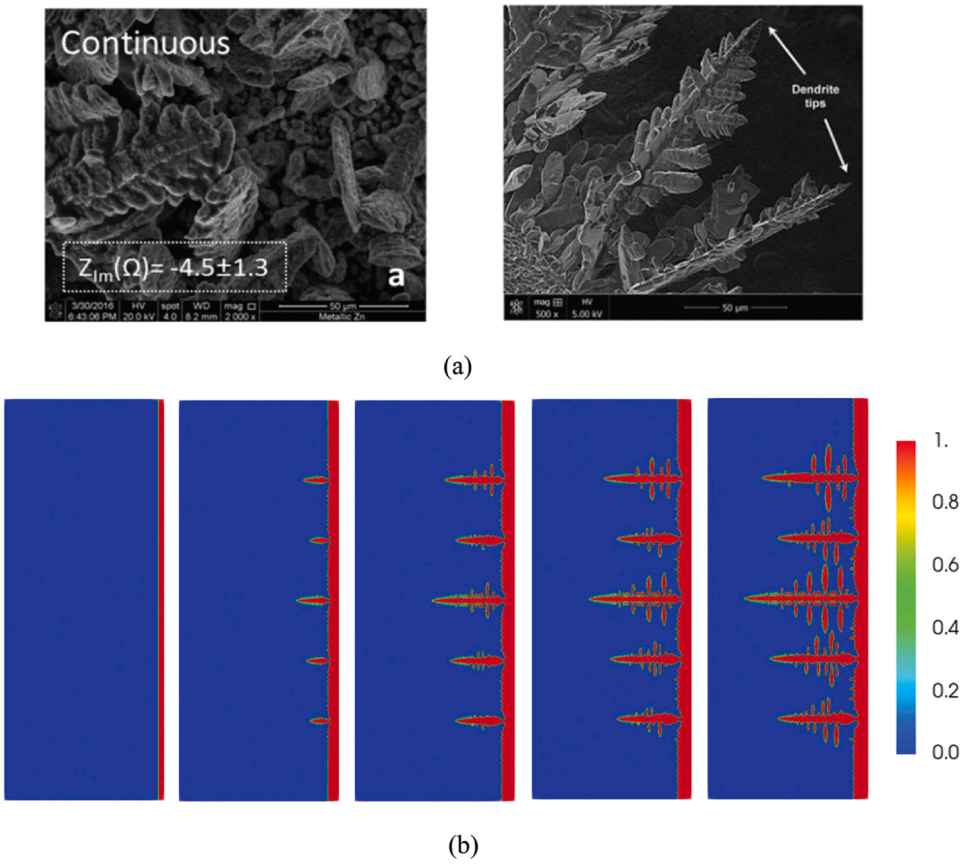

Fig. 11. (a) SEM image of zinc deposition phenomenon; (b) Dendrite evolution simulation at different charging times [147].

liquid, solid, and gas phases were established using the volume average method, similar to the HER in ZNB [142–144]. Huang et al. [115] developed a two-dimensional transient two-phase flow model for ZNB, considering the parasitic reaction of hydrogen evolution, to investigate the impact of the bubble flow formed by hydrogen bubbles and electrolytes on battery performance. Fig. 10 displays the concentration distribution of (a, b) OH^-, (c, d) $Zn(OH)_4^{2-}$under different SOC conditions under the condition that (a, c) considers bubble flow, and (b, d) does not consider bubble flow. (e) illustrates the variation of $OH^-$with SOC with/without bubble flow, while (f) illustrates the variation of $Zn(OH)_4^{2-}$ with SOC with/without bubble flow. The additional disturbance caused by bubble flow can effectively enhance ion transfer at the negative interface and reduce the loss of concentration/activation polarization. However, the current density distribution of negative interface HER and the negative main reaction is not uniform. This work provides the first mechanism explanation for the effect of two-phase flow induced by HER on ZNB performance.

The aforementioned research plays a significant role in comprehending side reactions in Zinc–Nickel single flow batteries. However, due to the differences in battery structure and reaction mechanisms, it is imperative to establish a multi-physical field coupling mechanism analysis model to gain insight into the side reaction of ZNB. Xu et al. [145,146] employed the LBM to develop the mechanism model of internal mass transfer and electrochemical reaction of the positive electrode and explored the distribution of ion concentration and reaction current density inside the ZNB. A 2-D numerical model of the porous electrode was subsequently established based on the positive structure of the porous electrode. The electrochemical reaction in porous electrodes was studied from the perspective of seepage and mass transfer in the pore. Then revealed a significant influence of proton concentration on reaction rate and current density, and a substantial impact of hydroxide concentration on over-potential. Yao et al. [147] also contributed to understanding ZNB by establishing a 2-D model that considered zinc dendrites using the phase field (PF) Lattice Boltzmann Method (PF-LBM). The evolution process of zinc dendrites and the spatial and temporal distribution of ions/electrons in batteries were studied. Fig. 11 presents the morphology and evolution of zinc dendrites after experimental and LBM simulation. The study showed that dendrite morphology can be altered by adjusting anisotropy intensity, leading to a reduction in dendrite formation. An increase in electrolyte flow rate was found to be beneficial in decreasing the ion concentration gradient on the cathode surface and increasing the ion diffusion rate. Luo et al. [148] utilized the quartet structure generation set (QSGS) method to reconstruct the microstructure of a porous nickel oxide electrode and simulated the flow mass transfer and the electrochemical reaction of porous electrode inside ZNB by LBM. For the first time, the effects of different porous electrode structures (porosity, particle size, and electrode thickness) on the charging performance and ion concentration distribution of ZNB were investigated from the perspective of pore permeability and transport properties. The results showed that decreased porosity and particle size leads to an increased diffusion rate of electrolyte ions and promotes electrochemical reaction under various pore structures. The augmentation of electrode thickness affects the diffusion of OH^- and intensifies concentration polarization, which is detrimental to the ZNB charging efficiency. Exploration of ZNB at micro and nano-scales is still nascent and holds significant implications for comprehending the influence of the internal structure on battery performance.

4.3. *Commercialization process*

Since its proposal in 2006, the Zinc–Nickel single flow battery has made significant advancements in large-scale domestic and

Table 4
Comparison of performance parameters of three generation products and improved products of ZNB [151].

Product number	Rated capacity	Rated voltage	Minimum cut-off voltage	Maximum cut-off voltage	Battery pairs	Positive and negative plate dimensions	Area capacity	Liquid supply mode	Cycle life/times	Coulomb efficiency /%
First generation	200 A h	1.6 V	1.2 V	2.05 V	15	150 × 180 mm	20 mA·h·cm^{-2}	External water pump	>10,000	>90 %
Second generation	216 A h	1.6 V	1.2 V	2.05 V	19	150 × 240 mm	20 mA·h·cm^{-2}	External water pump	>10,000	>90 %
Third generation	300 A h	1.6 V	1.2 V	2.05 V	23	150 × 240 mm	20 mA·h·cm^{-2}	Internal micropump	>10,000	>95 %
Third generation improved version	300 A h	1.6 V	1.2 V	2.05 V	23	150 × 240 mm	20 mA·h·cm^{-2}	External electrodes drive the propeller	>10,000	>95 %

international production. The battery has undergone extensive research and testing, including principle verification and small-scale pilot tests, resulting in a battery cycle life that exceeds 10,000 cycles. Currently, three generations of large-scale Zinc–Nickel single flow batteries have been developed, with the first generation being successfully produced by Zhejiang Yuyuan Energy Storage Technology Co., LTD [149]. The second generation battery production line is nearing completion, with 1 MW h capacity. Additionally, the China Zhangbei National Fengguang Energy Storage Demonstration Zone has established a ZNB energy storage system with a capacity of 50 KW·h, comprised of 168 200 A h single batteries in series, achieving an energy efficiency of 80 % [150]. The third generation battery, with 300 A h capacity, is currently undergoing optimization and improvement, showing promising prospects for application. Detailed performance parameters of the three generations of batteries and the improved products can be found in Table 4 [151].

Although the current Zinc–Nickel single flow battery has not been as close to commercial application as the all-vanadium flow battery, scholars have put forward great expectations for the engineering application prospects of the Zinc–Nickel single flow battery, and there will be more and more research focused on improving the performance of ZNB and large-scale application.

5. Conclusions

The Zinc–Nickel single flow battery (ZNB) offers numerous advantages, including high cycle life, low cost, and high efficiency. However, in its operational cycle, certain challenges such as capacity attenuation and efficiency reduction need to be investigated by further research into the internal mechanisms of the battery. This paper reviews the complete development process of ZNB and analyzes the current research situation and difficulties encountered. The following are some relevant conclusions and prospects:

(1) The study of ZNB involves a combination of experiments and numerical simulations to address challenges such as polarization loss, low energy density, and dendrite growth in batteries. Enhanced battery structures and materials with higher capacity are developed to overcome these issues. Using numerical simulations encompassing multiple physical fields, the internal mechanism and reaction principles of the ZNB are understood, and optimization methods are applied in the design process. The Lattice Boltzmann method is also utilized to investigate the impact of dendritic growth mechanisms and porous electrode structures on battery performance;
(2) The current numerical model for ZNB assumes homogeneity in the positive porous structure to simplify calculations and save time. However, this approach increases the errors of the model. The positive porous structure in ZNB affects mass transfer and electrolyte flow at the interface. Further investigation is needed to understand the effects of oxygen evolution, which occurs during the final stage of ZNB charging, on battery performance;
(3) The phenomenon of zinc dendrite growth in the negative electrode of the ZNB and the influence of hydrogen evolution reaction on battery operation requires additional research. Establishing a numerical model that considers the flow of hydrogen evolution bubbles and the growth of negative zinc dendrites is necessary. This would provide a more accurate understanding of dendrite growth and the mass transfer mechanism of negative electrodes in ZNB;
(4) The relationship between the mesoscopic electrode interface and the macroscopic bubble flow remains to be studied when the electrode precipitates gas. The current study considers the polarization process and its side effects for a single cycle. One potential future direction is to investigate the numerical process of the ZNB reactor and its operation over multiple cycles. This would greatly improve the specific engineering application process of the battery.

Declaration of Competing Interest

The authors declare that they have no known competing financial interests or personal relationships that could have appeared to influence the work reported in this paper.

Data availability

No data was used for the research described in the article.

Acknowledgments

This work was supported by Key Science and Technology Project of Xi'an (2021JH-QCY1-0052) and the Key Research and Development Project of Shaanxi Province (2022QCY-LL-25).

References

[1] Yan J. Energy systems in transition: challenges and opportunities. Adv Appl Energy 2021;1:100005.
[2] Liu K, Peng Q, Che Y, Zheng Y, Li K, Teodorescu R, Widanage D, Barai A. Transfer learning for battery smarter state estimation and ageing prognostics: recent progress, challenges, and prospects. Adv Appl Energy 2023;9:100117.
[3] Zhang H, Yan J. Co-benefits of renewable energy development: a brighter sky brings greater renewable power. Joule 2022;6:1142–4.
[4] Veers P, Dykes K, Lantz E, Barth S, Bottasso CL, Carlson O, Clifton A, Green J, Green P, Holttinen H, Laird D, Lehtomäki V, Lundquist JK, Manwell J, Marquis M, Meneveau C, Moriarty P, Munduate X, Muskulus M, Naughton J, Pao L, Paquette J, Peinke J, Robertson A, Sanz Rodrigo J, Sempreviva AM, Smith JC, Tuohy A, Wiser R. Grand challenges in the science of wind energy. Science 2019; 366:eaau2027.
[5] Hansen TA. Stranded assets and reduced profits: analyzing the economic underpinnings of the fossil fuel industry's resistance to climate stabilization. Renew Sustain Energy Rev 2022;158:112144.

[6] Hu K, Sinha A, Tan Z, Shah MI, Abbas S. Achieving energy transition in OECD economies: discovering the moderating roles of environmental governance. Renew Sustain Energy Rev 2022;168:112808.
[7] Zhang C, Yan J, You F. Critical metal requirement for clean energy transition: a quantitative review on the case of transportation electrification. Adv Appl Energy 2023;9:100116.
[8] Bouich A, Torres JC, Khattak YH, Baig F, Marí-Guaita J, Soucase BM, Mendez-Blas A, Palacios P. Bright future by controlling α/δ phase junction of formamidinium lead iodide doped by imidazolium for solar cells: insight from experimental, DFT calculations and SCAPS simulation. Surf Interfaces 2023;40:103159.
[9] Contino F, Moret S, Limpens G, Jeanmart H. Whole-energy system models: the advisors for the energy transition. Prog Energy Combust Sci 2020;81:100872.
[10] Notton G, Nivet ML, Voyant C, Paoli C, Darras C, Motte F, Fouilloy A. Intermittent and stochastic character of renewable energy sources: consequences, cost of intermittence and benefit of forecasting. Renew Sustain Energy Rev 2018;87:96–105.
[11] Rahman MM, Oni AO, Gemechu E, Kumar A. Assessment of energy storage technologies: a review. Energy Convers Manage 2020;223:113295.
[12] Huang WC, Zhang Q, You F. Impacts of battery energy storage technologies and renewable integration on the energy transition in the New York State. Adv Appl Energy 2023;9:100126.
[13] Zhang Z, Ding T, Zhou Q, Sun Y, Qu M, Zeng Z, Ju Y, Li L, Wang K, Chi F. A review of technologies and applications on versatile energy storage systems. Renew Sustain Energy Rev 2021;148:111263.
[14] Bouich A, Torres JC, Chfii H, Marí-Guaita J, Khattak YH, Baig F, Soucase BM, Palacios P. Delafossite as hole transport layer a new pathway for efficient perovskite-based solar sells: insight from experimental, DFT and numerical analysis. Sol Energy 2023;250:18–32.
[15] Dowling JA, Rinaldi KZ, Ruggles TH, Davis SJ, Yuan M, Tong F, Lewis NS, Caldeira K. Role of long-duration energy storage in variable renewable electricity systems. Joule 2020;4:1907–28.
[16] Jing R, Wang J, Shah N, Guo M. Emerging supply chain of utilizing electrical vehicle retired batteries in distributed energy systems. Adv Appl Energy 2021;1:100002.
[17] Lamnatou C, Chemisana D, Cristofari C. Smart grids and smart technologies in relation to photovoltaics, storage systems, buildings and the environment. Renew Energy 2022;185:1376–91.
[18] Bouich A, Marí-Guaita J, Soucase BM, Palacios P. Bright future by enhancing the stability of methylammonium lead triiodide perovskites thin films through Rb, Cs and Li as dopants. Mater Res Bull 2023;163:112213.
[19] Koohi-Fayegh S, Rosen MA. A review of energy storage types, applications and recent developments. J Energy Storage 2020;27:101047.
[20] Li X, Palazzolo A. A review of flywheel energy storage systems: state of the art and opportunities. J Energy Storage 2022;46:103576.
[21] Zhou Q, Du D, Lu C, He Q, Liu W. A review of thermal energy storage in compressed air energy storage system. Energy 2019;188:115993.
[22] Sun H, Zhu J, Baumann D, Peng L, Xu Y, Shakir I, Huang Y, Duan X. Hierarchical 3D electrodes for electrochemical energy storage. Nat Rev Mater 2019;4:45–60.
[23] He W, King M, Luo X, Dooner M, Li D, Wang J. Technologies and economics of electric energy storages in power systems: review and perspective. Adv Appl Energy 2021;4:100060.
[24] Xie J, Lu YC. A retrospective on lithium-ion batteries. Nat Commun 2020;11:2499.
[25] Moy K, Lee SB, Harris S, Onori S. Design and validation of synthetic duty cycles for grid energy storage dispatch using lithium-ion batteries. Adv Appl Energy 2021;4:100065.
[26] Qi L, Wang Y, Kong L, Yi M, Song J, Hao D, Zhou X, Zhang Z, Yan J. Manufacturing processes and recycling technology of automotive lithium-ion battery: a review. J Energy Storage 2023;67:107533.
[27] Patel JR, Rathod MK. Recent developments in the passive and hybrid thermal management techniques of lithium-ion batteries. J Power Sources 2020;480:228820.
[28] Zhang J, Shao D, Jiang L, Zhang G, Wu H, Day R, Jiang W. Advanced thermal management system driven by phase change materials for power lithium-ion batteries: a review. Renew Sustain Energy Rev 2022;159:112207.
[29] Tanim TR, Yang Z, Colclasure AM, Chinnam PR, Gasper P, Lin Y, Yu L, Weddle PJ, Wen J, Dufek EJ, Bloom I, Smith K, Dickerson CC, Evans MC, Tsai Y, Dunlop AR, Trask SE, Polzin BJ, Jansen AN. Extended cycle life implications of fast charging for lithium-ion battery cathode. Energy Storage Mater 2021;41:656–66.
[30] Ahniyaz A, de Meatza I, Kvasha A, Garcia-Calvo O, Ahmed I, Sgroi MF, Giuliano M, Dotoli M, Dumitrescu MA, Jahn M, Zhang N. Progress in solid-state high voltage lithium-ion battery electrolytes. Adv Appl Energy 2021;4:100070.
[31] Lopes PP, Stamenkovic VR. Past, present, and future of lead-acid batteries. Science 2020;369:923–4.
[32] Li M, Yang J, Liang S, Hou H, Hu J, Liu B, Kumar RV. Review on clean recovery of discarded/spent lead-acid battery and trends of recycled products. J Power Sources 2019;436:226853.
[33] Eng AYS, Kumar V, Zhang Y, Luo J, Wang W, Sun Y, Li W, Seh ZW. Room-temperature sodium–sulfur batteries and beyond: realizing practical high energy systems through anode, cathode, and electrolyte engineering. Adv Energy Mater 2021;11:2003493.
[34] Wang Y, Zhou D, Palomares V, Shanmukaraj D, Sun B, Tang X, Wang C, Armand M, Rojo T, Wang G. Revitalising sodium–sulfur batteries for non-high-temperature operation: a crucial review. Energy Environ Sci 2020;13:3848–79.
[35] Arenas LF, Ponce de León C, Walsh FC. Redox flow batteries for energy storage: their promise, achievements and challenges. Curr Opin Electrochem 2019;16:117–26.
[36] Yuan Z, Yin Y, Xie C, Zhang H, Yao Y, Li X. Advanced materials for zinc-based flow battery: development and challenge. Adv Mater 2019;31:1902025.
[37] Akram U, Nadarajah M, Shah R, Milano F. A review on rapid responsive energy storage technologies for frequency regulation in modern power systems. Renew Sustain Energy Rev 2020;120:109626.
[38] He X, Xiao G, Hu B, Tan L, Tang H, He S, He Z. The applications of energy regeneration and conversion technologies based on hydraulic transmission systems: a review. Energy Convers Manag 2020;205:112413.
[39] Salama HS, Vokony I. Comparison of different electric vehicle integration approaches in presence of photovoltaic and superconducting magnetic energy storage systems. J Clean Prod 2020;260:121099.
[40] Tong Z, Cheng Z, Tong S. A review on the development of compressed air energy storage in China: technical and economic challenges to commercialization. Renew Sustain Energy Rev 2021;135:110178.
[41] Pullen KR. The Status and Future of Flywheel Energy Storage. Joule 2019;3:1394–9.
[42] Zhang X, Li Z, Luo L, Fan Y, Du Z. A review on thermal management of lithium-ion batteries for electric vehicles. Energy 2022;238:121652.
[43] Yang Y, Wang R, Shen Z, Yu Q, Xiong R, Shen W. Towards a safer lithium-ion batteries: a critical review on cause, characteristics, warning and disposal strategy for thermal runaway. Adv Appl Energy 2023;11:100146.
[44] Wang Y, Wu X, Han Y, Li T. Flexible supercapacitor: overview and outlooks. J Energy Storage 2021;42:103053.
[45] Zhang Y, Zhou CG, Yang J, Xue SC, Gao HI, Yan XH, Huo QY, Wang SW, Cao Y, Yan J, Gao KZ, Wang LX. Advances and challenges in improvement of the electrochemical performance for lead-acid batteries: a comprehensive review. J Power Sources 2022;520:230800.
[46] Wang N, Wang Y, Bai Z, Fang Z, Zhang X, Xu Z, Ding Y, Xu X, Du Y, Dou S, Yu G. High-performance room-temperature sodium–sulfur battery enabled by electrocatalytic sodium polysulfides full conversion. Energy Environ Sci 2020;13:562–70.
[47] Zhang H, Lu W, Li X. Progress and perspectives of flow battery technologies. Electrochem Energy Rev 2019;2:492–506.
[48] Sun J, Wu M, Jiang H, Fan X, Zhao T. Advances in the design and fabrication of high-performance flow battery electrodes for renewable energy storage. Adv Appl Energy 2021;2:100016.
[49] Chen H, Zhang X, zhang s, Wu S, Chen F, Xu J. A comparative study of iron-vanadium and all-vanadium flow battery for large scale energy storage. Chem Eng J 2022;429:132403.
[50] Shin J, Jeong B, Chinannai MF, Ju H. Mitigation of water and electrolyte imbalance in all-vanadium redox flow batteries. Electrochim Acta 2021;390:138858.
[51] Huang Z, Mu A, Wu L, Yang B, Qian Y, Wang J. Comprehensive analysis of critical issues in all-vanadium redox flow battery. ACS Sustain Chem Eng 2022;10:7786–810.
[52] Vlasov VI, Gvozdik NA, Mokrousov MD, Ryazantsev SV, Luchkin SY, Gorin DA, Stevenson KJ. Ion-exchange membrane impact on preferential water transfer in all-vanadium redox flow battery. J Power Sources 2022;540:231640.
[53] Tempelman CHL, Jacobs JF, Balzer RM, Degirmenci V. Membranes for all vanadium redox flow batteries. J Energy Storage 2020;32:101754.
[54] Zhang L, Cheng J, Yang Y-s, Wen Y-h, Wang X-d, Cao G-p. Study of zinc electrodes for single flow zinc/nickel battery application. J Power Sources 2008;179:381–7.
[55] Li S, Li K, Xiao E, Zhang J, Zheng M. Real-time peak power prediction for zinc nickel single flow batteries. J Power Sources 2020;448:227346.
[56] Zhou R, Yao S, Zhao Y, Cheng J. Tab design based on the internal distributed properties in a zinc–nickel single-flow battery. Ind Eng Chem Res 2021;60:1434–51.
[57] Esan OC, Shi X, Pan Z, Huo X, An L, Zhao T. Modeling and simulation of flow batteries. Adv Energy Mater 2020;10:2000758.
[58] Thaller LH. Electrically rechargeable redox flow cells. In: 9th Intersociety Energy Conversion Engineering Conference; 1974. p. 924–8.
[59] Sánchez-Díez E, Ventosa E, Guarnieri M, Trovò A, Flox C, Marcilla R, Soavi F, Mazur P, Aranzabe E, Ferret R. Redox flow batteries: status and perspective towards sustainable stationary energy storage. J Power Sources 2021;481:228804.
[60] Amit L, Naar D, Gloukhovski R, la O GJ, Suss ME. A single-flow battery with multiphase flow. ChemSusChem 2021;14:1068–73.
[61] Johnson DA, Reid MA. Chemical and electrochemical behavior of the Cr(III)/Cr(II) Half-cell in the iron-chromium redox energy storage system. J Electrochem Soc 1985;132:1058.
[62] M. Shimada, Y. Tsuzuki, Y. Iizuka, M. Inoue, Investigation of the aqueous Fe-Cr redox flow cell, 3 (1988).
[63] Bae CH, Roberts EPL, Dryfe RAW. Chromium redox couples for application to redox flow batteries. Electrochim Acta 2002;48:279–87.
[64] Lopez-Atalaya M, Codina G, Perez JR, Vazquez JL, Aldaz A. Optimization studies on a Fe/Cr redox flow battery. J Power Sources 1992;39:147–54.
[65] Skyllas-Kazacos M, Rychcik M, Robins RG, Fane AG, Green MA. New all-vanadium redox flow cell. J Electrochem Soc 1986;133:1057.
[66] Zhang H, Li X, Zhang J. Redox flow batteries: fundamentals and applications. CRC Press; 2017.
[67] Rychcik M, Skyllas-Kazacos M. Evaluation of electrode materials for vanadium redox cell. J Power Sources 1987;19:45–54.

[68] Rychcik M, Skyllas-Kazacos M. Characteristics of a new all-vanadium redox flow battery. J Power Sources 1988;22:59–67.
[69] Zhong S, Skyllas-Kazacos M. Electrochemical behaviour of vanadium(V)/vanadium(IV) redox couple at graphite electrodes. J Power Sources 1992;39:1–9.
[70] Kausar N, Howe R, Skyllas-Kazacos M. Raman spectroscopy studies of concentrated vanadium redox battery positive electrolytes. J Appl Electrochem 2001;31:1327–32.
[71] Chieng SC, Kazacos M, Skyllas-Kazacos M. Preparation and evaluation of composite membrane for vanadium redox battery applications. J Power Sources 1992;39:11–9.
[72] Mohammadi T, Kazacos MS. Modification of anion-exchange membranes for vanadium redox flow battery applications. J Power Sources 1996;63:179–86.
[73] Sukkar T, Skyllas-Kazacos M. Membrane stability studies for vanadium redox cell applications. J Appl Electrochem 2004;34:137–45.
[74] Skyllas-Kazacos M, Peng C, Cheng M. Evaluation of precipitation inhibitors for supersaturated vanadyl electrolytes for the vanadium redox battery. Electrochem Solid State Lett 1999;2:121.
[75] Sun B, Skyllas-Kazakos M. Chemical modification and electrochemical behavior of graphite fiber in acidic vanadium solution. Electrochim Acta 1991;36:513–7.
[76] Sun B, Skyllas-Kazacos M. Modification of graphite electrode materials for vanadium redox flow battery application—I. Thermal treatment. Electrochim Acta 1992;37:1253–60.
[77] Sun B, Skyllas-Kazacos M. Chemical modification of graphite electrode materials for vanadium redox flow battery application—Part II. Acid treatments. Electrochim Acta 1992;37:2459–65.
[78] Zhong S, Padeste C, Kazacos M, Skyllas-Kazacos M. Comparison of the physical, chemical and electrochemical properties of rayon- and polyacrylonitrile-based graphite felt electrodes. J Power Sources 1993;45:29–41.
[79] Sharifi B, Mojtahedi M, Goodarzi M, Vahdati Khaki J. Effect of alkaline electrolysis conditions on current efficiency and morphology of zinc powder. Hydrometallurgy 2009;99:72–6.
[80] Sukkar T, Skyllas-Kazacos M. Water transfer behaviour across cation exchange membranes in the vanadium redox battery. J Membr Sci 2003;222:235–47.
[81] Sukkar T, Skyllas-Kazacos M. Modification of membranes using polyelectrolytes to improve water transfer properties in the vanadium redox battery. J Membr Sci 2003;222:249–64.
[82] Sun CN, Delnick FM, Baggetto L, Veith GM, Zawodzinski TA. Hydrogen evolution at the negative electrode of the all-vanadium redox flow batteries. J Power Sources 2014;248:560–4.
[83] Chen F, Liu J, Chen H, Yan C. Study on hydrogen evolution reaction at a graphite electrode in the all-vanadium redox flow battery. Int J Electrochem Sci 2012;7:3750–64.
[84] Chen F, Gu S, Ma Q, Liu Q, Zhang M. Vanadium (III)/Vanadium (II) and hydrogen evolution thermodynamic behavior at the negative of the all-vanadium redox flow batteries. J Electrochem Soc 2017;164:A2403.
[85] Kim KJ, Lee HS, Kim J, Park MS, Kim JH, Kim YJ, Skyllas-Kazacos M. Superior electrocatalytic activity of a robust carbon-felt electrode with oxygen-rich phosphate groups for all-vanadium redox flow batteries. ChemSusChem 2016;9:1329–38.
[86] Taylor SM, Pătru A, Perego D, Fabbri E, Schmidt TJ. Influence of carbon material properties on activity and stability of the negative electrode in vanadium redox flow batteries: a model electrode study. ACS Appl Energy Mater 2018;1:1166–74.
[87] Mehboob S, Ali G, Abbas S, Chung KY, Ha HY. Elucidating the performance-limiting electrode for all-vanadium redox flow batteries through in-depth physical and electrochemical analyses. J Ind Eng Chem 2019;80:450–60.
[88] Eifert L, Jusys Z, Behm RJ, Zeis R. Side reactions and stability of pre-treated carbon felt electrodes for vanadium redox flow batteries: a DEMS study. Carbon N Y 2020;158:580–7.
[89] Schweiss R, Pritzl A, Meiser C. Parasitic hydrogen evolution at different carbon fiber electrodes in vanadium redox flow batteries. J Electrochem Soc 2016;163:A2089.
[90] Vázquez-Galván J, Flox C, Fàbrega C, Ventosa E, Parra A, Andreu T, Morante JR. Hydrogen-treated rutile TiO2 shell in graphite-core structure as a negative electrode for high-performance vanadium redox flow batteries. ChemSusChem 2017;10:2089–98.
[91] Derr I, Fetyan A, Schutjajew K, Roth C. Electrochemical analysis of the performance loss in all vanadium redox flow batteries using different cut-off voltages. Electrochim Acta 2017;224:9–16.
[92] Gahn RF, Hagedorn NH, Johnson JA. Cycling performance of the iron-chromium redox energy storage system. NASA Lewis Research Center, Cleveland, OH (United States); 1985.
[93] Zeng Y, Zhao T, Zhou X, Zou J, Ren Y. A hydrogen-ferric ion rebalance cell operating at low hydrogen concentrations for capacity restoration of iron-chromium redox flow batteries. J Power Sources 2017;352:77–82.
[94] Jayathilake B, Plichta E, Hendrickson M, Narayanan S. Improvements to the coulombic efficiency of the iron electrode for an all-iron redox-flow battery. J Electrochem Soc 2018;165:A1630.
[95] Pletcher D, Wills R. A novel flow battery: a lead acid battery based on an electrolyte with soluble lead (II) Part II. Flow cell studies. Phys Chem Chem Phys 2004;6:1779–85.
[96] WEN YH, GAO C, CHENG J, PAN JQ, CAO GP, YANG YS. Effect of electrolyte on the performance of electrodes for an all lead flow battery. Acta Phys Chim Sin 2013;29:2354–60.
[97] Oury A, Kirchev A, Bultel Y. Oxygen evolution on alpha-lead dioxide electrodes in methanesulfonic acid. Electrochim Acta 2012;63:28–36.
[98] Naziris A, Guarderas G, Francés A, Asensi R, Uceda J. Large-signal black-box modelling of bidirectional battery charger for electric vehicles. In: 2019 IEEE Applied Power Electronics Conference and Exposition (APEC); 2019. p. 3195–8.
[99] Feng F, Teng S, Liu K, Xie J, Xie Y, Liu B, Li K. Co-estimation of lithium-ion battery state of charge and state of temperature based on a hybrid electrochemical-thermal-neural-network model. J Power Sources 2020;455:227935.
[100] Nejad S, Gladwin DT, Stone DA. A systematic review of lumped-parameter equivalent circuit models for real-time estimation of lithium-ion battery states. J Power Sources 2016;316:183–96.
[101] Li M, Hikihara T. A coupled dynamical model of redox flow battery based on chemical reaction, fluid flow, and electrical circuit. IEICE Trans Fundam Electron Commun Comput Sci 2008;91:1741–7.
[102] Shah A, Watt-Smith M, Walsh F. A dynamic performance model for redox-flow batteries involving soluble species. Electrochim Acta 2008;53:8087–100.
[103] Al-Fetlawi H, Shah A, Walsh F. Non-isothermal modelling of the all-vanadium redox flow battery. Electrochim Acta 2009;55:78–89.
[104] You D, Zhang H, Sun C, Ma X. Simulation of the self-discharge process in vanadium redox flow battery. J Power Sources 2011;196:1578–85.
[105] Ma X, Zhang H, Xing F. A three-dimensional model for negative half cell of the vanadium redox flow battery. Electrochim Acta 2011;58:238–46.
[106] Tang A, Bao J, Skyllas-Kazacos M. Thermal modelling of battery configuration and self-discharge reactions in vanadium redox flow battery. J Power Sources 2012;216:489–501.
[107] Zheng Q, Zhang H, Xing F, Ma X, Li X, Ning G. A three-dimensional model for thermal analysis in a vanadium flow battery. Appl Energy 2014;113:1675–85.
[108] Wang F, Xiao G, Chu F. Mass transfer enhancement in electrode and battery performance optimization of all-vanadium flow based on channel section reconstruction. Chem Eng J 2023;451:138619.
[109] Al-Fetlawi H, Shah A, Walsh F. Modelling the effects of oxygen evolution in the all-vanadium redox flow battery. Electrochim Acta 2010;55:3192–205.
[110] Shah A, Al-Fetlawi H, Walsh F. Dynamic modelling of hydrogen evolution effects in the all-vanadium redox flow battery. Electrochim Acta 2010;55:1125–39.
[111] M. Manninen, V. Taivassalo, S. Kallio, On the mixture model for multiphase flow, (1996).
[112] Wang H, Leung DY, Leung MK, Ni M. Modeling of parasitic hydrogen evolution effects in an aluminum– air cell. Energy Fuels 2010;24:3748–53.
[113] Zhou C, Bhonge K, Cho KT. Analysis of the effect of hydrogen-evolving side reaction in the aqueous aluminum-air battery. Electrochim Acta 2020;330:135290.
[114] Lao-Atiman W, Bumroongsil K, Arpornwichanop A, Bumroongsakulsawat P, Olaru S, Kheawhom S. Model-based analysis of an integrated zinc-air flow battery/zinc electrolyzer system. Front Energy Res 2019;7:15.
[115] Huang X, Yao S, Zhou R, Yang X, Kan X, Cheng J. Study on the effect of hydrogen evolution reaction in the Zinc–Nickel single flow battery. J Energy Storage 2022;50:104246.
[116] Yao S, Zhou R, Huang X, Liu D, Cheng J. Three-dimensional transient model of Zinc–Nickel single flow battery considering side reactions. Electrochim Acta 2021;374:137895.
[117] Cheng J, Zhang L, Yang YS, Wen YH, Cao GP, Wang XD. Preliminary study of single flow zinc–nickel battery. Electrochem Commun 2007;9:2639–42.
[118] Cheng J, Wen YH, Xu Y, Cao GP, Yang YS. Effect of matrix on electrodeposition of zinc in flowing potassium zincate lye. Chem J High Educ 2011;32:2640–4.
[119] Cheng J, Wen YH, Cao GP, Yang YS. Influence of zinc ions in electrolytes on the stability of nickel oxide electrodes for single flow zinc–nickel batteries. J Power Sources 2011;196:1589–92.
[120] Wen Y, Wang T, Cheng J, Pan J, Cao G, Yang Y. Lead ion and tetrabutylammonium bromide as inhibitors of the growth of spongy zinc in single flow zinc/nickel batteries. Electrochim Acta 2012;59:64–8.
[121] Cheng Y, Zhang H, Lai Q, Li X, Shi D. Performance gains in single flow zinc–nickel batteries through novel cell configuration. Electrochim Acta 2013;105:618–21.
[122] Cheng Y, Lai Q, Li X, Xi X, Zheng Q, Ding C, Zhang H. Zinc–Nickel single flow batteries with improved cycling stability by eliminating zinc accumulation on the negative electrode. Electrochim Acta 2014;145:109–15.
[123] Cheng Y, Zhang H, Lai Q, Li X, Shi D, Zhang L. A high power density single flow zinc–nickel battery with three-dimensional porous negative electrode. J Power Sources 2013;241:196–202.
[124] Cheng Y, Zhang H, Lai Q, Li X, Zheng Q, Xi X, Ding C. Effect of temperature on the performances and in situ polarization analysis of zinc–nickel single flow batteries. J Power Sources 2014;249:435–9.
[125] Cheng Y, Xi X, Li D, Li X, Lai Q, Zhang H. Performance and potential problems of high power density zinc–nickel single flow batteries. RSC Adv 2015;5:1772–6.
[126] Ito Y, Nyce M, Plivelich R, Klein M, Banerjee S. Gas evolution in a flow-assisted zinc–nickel oxide battery. J Power Sources 2011;196:6583–7.
[127] Dundálek J, Šnajdr I, Libánský O, Vrána J, Pocedič J, Mazúr P, Kosek J. Zinc electrodeposition from flowing alkaline zincate solutions: role of hydrogen evolution reaction. J Power Sources 2017;372:221–6.
[128] Wang T, Yang M, Pan J. A new single flow Zinc–Nickel hybrid battery using a Ni (OH) 2-O2 composite cathode. Int J Electrochem Sci 2017;12:6022–30.
[129] Liu X, Xie Z, Cheng J, Zhao P, Gu W. Mathematical modeling of the nickel electrode for the single flow Zinc–Nickel battery, 2009 world non-grid-connected wind power and energy conference. IEEE; 2009. p. 1–4.
[130] Xiao M, Wang Y, Yao S, Song Y, Cheng J, He K. Analysis of internal reaction and mass transfer of Zinc–Nickel single flow battery. J Renew Sustain Energy 2016;8:064102.

[131] Yao S, Liao P, Xiao M, Cheng J, He K. Modeling and simulation of the Zinc–Nickel single flow batteries based on MATLAB/Simulink. AIP Adv 2016;6:125302.
[132] Yao S, Liao P, Xiao M, Cheng J, He K. Equivalent circuit modeling and simulation of the zinc nickel single flow battery. AIP Adv 2017;7:055112.
[133] Yao S, Sun X, Xiao M, Cheng J, Shen Y. Equivalent circuit model construction and dynamic flow optimization based on zinc–nickel single-flow battery. Energies 2019;12:582.
[134] Yao S, Zhao Y, Sun X, Ding D, Cheng J. Numerical studies of cell stack for Zinc–Nickel single flow battery. Int J Electrochem Sci 2019:14.
[135] Yao S, Zhao Y, Sun X, Zhao Q, Cheng J. A dynamic model for discharge research of Zinc–Nickel single flow battery. Electrochim Acta 2019;307:573–81.
[136] Yao S, Huang X, Sun X, Zhou R, Cheng J. Structural modification of negative electrode for zinc–nickel single–flow battery based on polarization analysis. J Electrochem Soc 2021;168:070512.
[137] Huang X, Yao S, Yang X, Sun X, Zhou R, Liu X, Cheng J. Polarization analysis and optimization of negative electrode nickel foam structure of Zinc–Nickel single-flow battery. J Energy Storage 2022;55:105624.
[138] Yao S, Sun X, Chen Y, Xiao M, Cheng J, Shen Y. Two-dimensional transient model and mechanism of the self-discharging of zinc–nickel single-flow batteries. J Renew Sustain Energy 2019;11:024105.
[139] De Vidts P, White RE. Mathematical modeling of a nickel-cadmium cell: proton diffusion in the nickel electrode. J Electrochem Soc 1995;142:1509.
[140] De Vidts P, Delgado J, White RE. A multiphase mathematical model of a nickel/hydrogen cell. J Electrochem Soc 1996;143:3223.
[141] De Vidts P, White RE. Governing equations for transport in porous electrodes. J Electrochem Soc 1997;144:1343.
[142] Vogt H. On the supersaturation of gas in the concentration boundary layer of gas evolving electrodes. Electrochim Acta 1980;25:527–31.
[143] Crowe CT. On models for turbulence modulation in fluid–particle flows. Int J Multiph Flow 2000;26:719–27.
[144] Kuzmin D, Turek S. Finite element discretization tools for gas-liquid flows. Bubbly Flows 2004:191–201.
[145] Yao SG, Xu LK, Li Y, Cheng J. Pore-scale simulation of internal reaction mechanism of positive electrode for Zinc–Nickel single-flow battery. J Solid State Electrochem 2020;24:915–28.
[146] Yao SG, Xu LK, Sun ZY, Cheng J. Electrochemical mechanism in porous electrode of zinc–nickel single-flow battery based on lattice Boltzmann method. Int J Heat Mass Transf 2019;138:903–15.
[147] Yao S, Kan X, Zhou R, Ding X, Xiao M, Cheng J. Simulation of dendritic growth of a zinc anode in a zinc–nickel single flow battery using the phase field-lattice Boltzmann method. New J Chem 2021;45:1838–52.
[148] Luo J, Yao S, Liu R, Kan X, Yang Y, Cheng J. Study on ion transport mechanism of Zinc–Nickel single-flow battery with different porous electrode structures based on lattice Boltzmann method. J Electrochem Soc 2022;169:050518.
[149] Li Y, Li K, Li S, Li Y. FRA and EKF based state of charge estimation of Zinc–Nickel single flow batteries. Advances in green energy systems and smart grid: first international conference on intelligent manufacturing and internet of things and 5th international conference on computing for sustainable energy and environment, IMIOT and ICSEE 2018, Chongqing, China, September 21-23, 2018, proceedings, Part III 5. Springer; 2018. p. 183–91.
[150] Lin X, Guo Y. A dynamic model of single flow Zinc-Nickle battery, 2015 Chinese Automation Congress (CAC). IEEE; 2015. p. 1328–32.
[151] Yang Z, Lou J, Li X, Wang H, Wang K, You D. Development status of Zinc–Nickel single flow battery. Energy Storage Sci Technol 2020;9:1678–90.